Effects of Boundary Conditions on Magnetic Friction

Kentaro Sugimoto
Department of Physics, The University of Tokyo

January 30, 2018

I would like to thank Prof. Hatano for useful discussions. I am grateful to Dr. Hinokihara in the Miyashita group, Department of Physics, the University of Tokyo, for sharing his expertise on the parallel computing techniques. I also thank Dr. Tamura, National Institute for Material Science, for useful comments on precursors of critical phenomena in finite-size systems. I would also like to express my gratitude to the members of the Hatano group and my family for their moral support and warm encouragements.

Abstract

We numerically investigate magnetic friction in the non-equilibrium Ising model with the quasi-one-dimensional geometry. The upper half of the system slides against the lower half along the transverse axis with a fixed sliding velocity. We calculate the frictional force density and the bulk energy density. We find peaks in their temperature derivatives, which may diverge in the two-dimensional limit. The result is consistent with Ref. [1], which showed a novel boundary critical temperature higher than the ordinary bulk critical point in two dimensions.

Contents

Chapter 1

Introduction

From old days, frictional forces between two solid-state matters have been thought to obey the following three fundamental laws—the Amontons-Coulomb law [2]:

1. The frictional force is independent of the size of the *apparent* contact area;
2. The frictional force is proportional to the normal force on the sliding body;
3. The dynamic frictional force is independent of the sliding velocity and is less than the static one.

The former two laws hold irrespective of static or dynamic force. These two laws imply that the frictional coefficient, defined by the ratio of the frictional force and the load of the sliding body, is a constant.

However, it began to be known that several experimental facts violate the Amontons-Coulomb law, particularly the third law about the velocity independence, depending on system parameters such as the temperature [3–7]. The velocity dependence of the friction shows, in general, quite different aspects for regions of very large velocities and very small ones.

A new wider framework of frictional forces, called the *constitutive equation of friction* [8], is thought to cover the frictional phenomena irrespectively of whether the Amontons-Coulomb law holds or not. The constitutive equation of friction improves the third law, describing the velocity dependence of the frictional force. This framework assumes that the frictional coefficient obeys the following form:

$$\mu = \mu_0 + A \log \left[1 + \frac{v}{v_0} \right] + B \log \left[1 + \frac{\theta}{\theta_0} \right], \tag{1.1}$$

where A, B, v_0 and θ_0 are constants, while v and θ denote the sliding velocity and a *state variable*, respectively. The constitutive equation of motion, as obvious from its form, describes the logarithmic dependence of the frictional coefficient on the velocity. We generally impose the constraint $d\theta/dt = 1 - \theta v/D_\mathrm{c}$ on the variables v and θ, where D_c is a constant. If we make the sliding object have a constant velocity v the time dependences of v and θ vanish and the relation $D_\mathrm{c} = \theta v$ always holds, and hence the coefficient behaves as $\mu = \text{const.} + (A - B) \log v$ in the regime sufficiently large velocity. This framework includes other parameters such as the temperature in a natural manner.

From the viewpoint of the interaction, we understand the velocity dependence of the friction in the following way. We consider an object O and a substrate S, letting O slide against S by applying an external force $F_{\rm ext}$ to O. When O and S interact with each other, the kinetic energy of O given by the external force is expected to be lost through the interaction, and then the entire system of O and S heats up (if the system is closed) or the energy dissipates from the system to an external environment (if the system is open). In the latter case, when we control the external force $F_{\rm ext}$ to balance it with the frictional force $F_{\rm fric}$ the sliding velocity v becomes constant and the dissipation process becomes stationary. Then the frictional force $F_{\rm fric}$ can be considered as a function of the sliding velocity v. If we set the temperature of the environment constant, we can also discuss the temperature dependence in the stationary regime of an open system.

It is also important to understand macroscopic frictional phenomena by fundamental laws of microscopic physical degrees of freedom. Nonetheless, many conventional ways of statistical mechanics are not applicable directly to the frictional phenomena. For example, the linear-response theory appears to solve the problem if the velocity v is much smaller than the rate ξ/τ, where ξ and τ are the characteristic length and time of the system, respectively. However, we already know well that the static frictional force is non-zero for many systems, for which the frictional force has a non-linear velocity dependence. This shows us that the complexity of the problem is beyond the linear-response theory.

For this reason, many theoretical researches on frictional phenomena have been performed by means of numerical simulations and approximately solvable models. For example, sliding frictions with a logarithmic dependence on the velocity have been investigated in terms of the Prandtl-Tomlinson model, which describes a total stick-slip motion as an elementary process [**Sang2001**, 6, 9–12]. As a many-body description of the stick-slip motion, researches using the Frenkel-Kontrova model also has been performed [7, 13–15]. A novel frictional phenomenon of vanishing frictional force, namely *superlubricity*, is well understood by the Frenkel-Kontrova model [16, 17].

Frictional phenomena are not captured only by classical picture, such as a moving mass interacts with a sinusoidal potential. In recent researches, the contribution of conduction electrons in superconductors to the friction (**electronic friction**) found to drop abruptly near the superconducting $T_{\rm c}$ [18–20] and that of localized spins in magnetic materials (**magnetic friction**) was investigated by numerical methods for macroscopic systems [21–23] and observed by the scanning tunneling microscopy [24].

In the present work we focus on the spin degrees of freedom and introduce a new viewpoint of manipulating the friction by an external operation. General ways of manipulating the friction in the scales of atoms and molecules have been already discussed. However, almost all of them are limited to mechanical ways, such as reducing the actual load to realize a smaller normal force and using intrinsic properties of the system such as the superlubricity. In contrast, we use the boundary conditions as an effective field which couples directly with the spin degrees of freedom in order to control the frictional force. Our way of manipulating the friction is applicable not only to spin systems but widely to electron systems and so on, opening up a new way of manipulating the friction.

The setup is in the following way. We consider two strips of the quasi-one-dimensional Ising model sliding against each other with a fixed velocity. Note that we assume the perfectly contacting two bodies, which produces the frictional force proportional to the contact area, and consider the dynamical friction (hereinafter simply called "friction")

in a stationary regime far from equilibrium. We discuss the difference of the frictional forces under two boundary conditions, namely the anti-parallel and the parallel, and its dependence on the distance between the two boundaries. We show a relation between the manipulativeness of the magnetic friction and the dimensionality of the system. In the one-dimensional limit the boundary conditions seem to have the maximum effect on the friction, whereas in the two-dimensional limit there seems to be no effects.

This paper is organized as follows. In a brief review in Chapter 2, we provides the fact that Ising models with any spatial dimension and geometry have a non-equilibrium phase transition, which occurs generally at a higher temperature than its equilibrium case. Chapter 3 provides the setup of our model in detail and definitions of physical quantities in both the non-equilibrium regime and the equilibrium one. In Chapter 4, we discuss the results from our simulation in association with the non-equilibrium phase transitions in Chapter 2. Our conclusions are summarized in Chapter 5.

Chapter 2

Velocity-driven Non-equilibrium Phase Transition in Ising Models

Two moving magnets sometimes gain their magnetic orders at a higher temperature than its equilibrium case. Using an exactly solvable model, Hucht [1] showed the existence of non-equilibrium phase transitions in Ising spin systems, which strongly depended on their spatial dimensionality. It is necessary to understand these non-equilibrium phase transitions for specific spatial dimensionality because manipulating the magnetic friction strongly depends on it. We will find a dimensional crossover of the friction in Chap. 4.

In this chapter we make a brief review of the exact results by Hucht [1]. His analysis is based on the fact that two Ising cylinders with relative motion make a novel mean field, which leads the system to a non-trivial phase transition.

2.1 Overview of the results

Let us consider two equivalent square lattices of the Ising model each of which contacts the other by one of its one-dimensional boundaries (see Fig. 2.1). We make one lattice slide along the contact plane against the other lattice with a constant velocity v. The entire system thereby goes into a non-equilibrium stationary state instead of equilibrium. The stationary state well describes the behavior of two magnetic materials with a friction. We use this setup in Chapter 3.

As a well known fact, the ordinary two-dimensional Ising model has an equilibrium phase transition at the critical temperature $T_{\mathrm{c,eq}} = 2/\left[\log\left(1+\sqrt{2}\right)\right] = 2.2691853\ldots$ in the thermodynamical limit. The system with the friction reduces to the equilibrium case in the limit of $v \to 0$. For finite velocity, it was revealed [1, 21] that there exists above the equilibrium critical point a novel phase transition in which the magnetization grows on the sliding boundary (see Fig. 2.2). Let us denote the velocity-dependent non-equilibrium critical point by $T_{\mathrm{c}}(v)$ apart from the equilibrium critical point $T_{\mathrm{c,eq}}$. Hucht [1] claimed that the critical temperature $T_{\mathrm{c}}(v)$ *deviates* from $T_{\mathrm{c,eq}}$ at the point $v = 0$ towards the limit $v = \infty$.

This phenomenon was first reported by Kadau *et al.* [21], who used Monte Carlo simulations both with the Metropolis and the Glauber algorithms in a two-dimensional model, and then was investigated in a more analytic manner by Hucht [1] in several dimensionalities and model geometries. One of the important points of the latter result

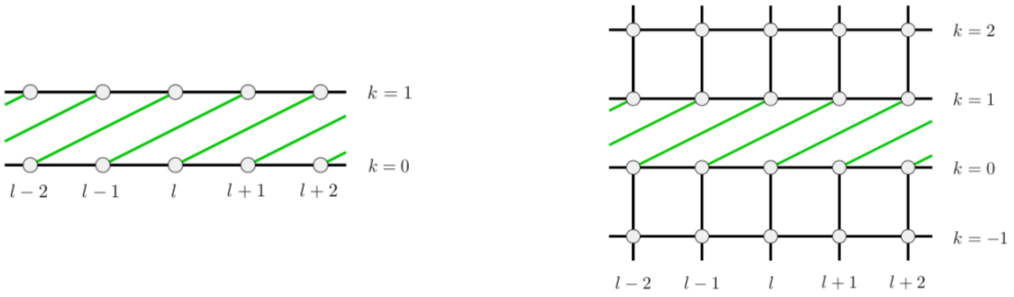

(a) (b)

Figure 2.1: Sketches of the models considered in Ref. [1]. Both cases depict a schematic view after the sliding by twice a lattice constant: (a) Two chains of the one-dimensional model; (b) Two square lattices of the two-dimensional model. Letters k and l denote the coordinates on z and x axes, respectively. Reprinted Figs. 2 and 3 with permission from A. Hucht, Phys. Rev. E **80**, 061138 (2009). Copyright (2018) by the American Physical Society.

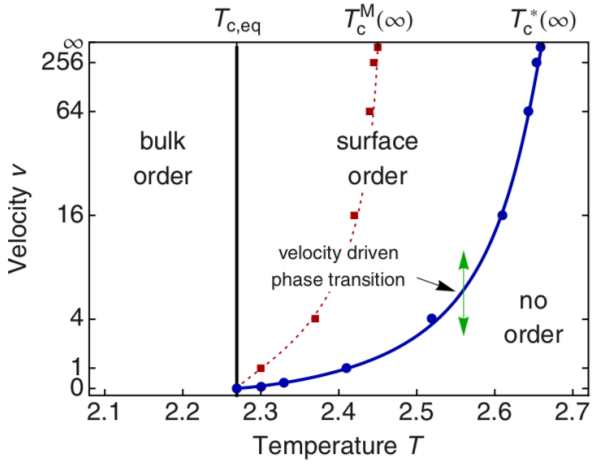

Figure 2.2: The phase diagram of the two-dimensional non-equilibrium Ising model obtained in Ref. [1]. The black solid line, the red dashed line and the blue solid line indicate the ordinary bulk phase transition $T_{\mathrm{c,eq}}$, a non-equilibrium boundary phase transition for the Metropolis rate $T_{\mathrm{c}}^{\mathrm{M}}(v)$ and one for the multiplicative rate $T_{\mathrm{c}}^{*}(v)$, respectively. Crossing from the right to the left across the non-equilibrium phase boundary, the system acquires a non-zero expectation value of magnetization on the sliding boundary. Reprinted Fig. 15 with permission from A. Hucht, Phys. Rev. E **80**, 061138 (2009). Copyright (2018) by the American Physical Society.

is that a mean field analysis becomes exact for the *second* critical temperature in the limit $v \to \infty$ when we use a novel algorithm called the *multiplicative rate*; this critical temperature is indicated as $T_c^*(\infty)$ in Fig. 2.2. The use of the multiplicative rate also produced an exact equation for $T_c^*(v)$, which depends on the flip rate and the sliding velocity $v > 0$. Hucht additionally obtained the line $T_c^{\mathrm{M}}(v)$ for the Metropolis rate numerically, which we will compare with our result in Chapter 4.

We can expect the system to behave similarly to its equilibrium state, if the velocity v is much less than the rate $\xi_x^{(\mathrm{eq})}(\beta)/\tau_x^{(\mathrm{eq})}(\beta)$, where $\xi_x^{(\mathrm{eq})}(\beta)$ and $\tau_x^{(\mathrm{eq})}(\beta)$ are the correlation length along the direction parallel to the sliding surface and the correlation time, respectively, for the equilibrium state at an inverse temperature $\beta := (k_{\mathrm{B}}T)^{-1}$. This corresponds to the case in which the pumped energy by the constant sliding quickly relaxes into the heat bath and the structure of domain walls near the sliding boundary is well sustained. On the other hand, the velocity v much greater than the rate $\xi_x^{(\mathrm{eq})}(\beta)/\tau_x^{(\mathrm{eq})}(\beta)$ should lead the system to a stationary state far from equilibrium, so that the structure near the sliding boundary is destroyed.

In the latter case a mean field picture [1] well describes the behavior of the system; a set of the moving spins along the contact plane act on the other set of *relatively* moving spins as a spatially averaged effective field. It turns out that the self-consistent equation gives the exact critical temperature $T_c^*(\infty)$ [1].

2.2 Concrete Examples: One-dimension and Two-dimension

We summarize the result for one-dimensional chains and two-dimensional planes in order to discuss the crossover from one dimension to two dimensions in our models in Chapter 4. We first give a general Hamiltonian of the Ising model as follows:

$$\mathcal{H}_\mu := -J\sum_{i<j}\sigma_i\sigma_j - h^{\mathrm{ext}}\sum_i \sigma_i - J\sum_i \mu_i\sigma_i, \tag{2.1}$$

where J, h^{ext} and μ_i with $\mu_i = \pm 1$ denote the exchange interaction, an external field and a stochastic field on the ith spin, respectively. The geometry of the model is either Fig. 2.1 (a) or (b). When the upper half moves rapidly against the lower half, the spins on one boundary may work on the spins on the other boundary only stochastically. The field μ_i represents this effect. Let us denote the stochastic average with respect to $\{\mu_i\}$ by $\langle\bullet\rangle_\mu$. We assume that μ_i obeys a probability distribution $p_i(\mu_i)$ such that $\langle\mu_i\rangle_\mu = m_{\mathrm{b}}$ for a given value of the boundary magnetization m_{b}, with the definition $\langle A_i\rangle_\mu := \sum_{\mu_i=\pm1} p(\mu_i)_i A_i$ for an arbitrary variable A_i. The form $p_i(\mu_i) := (1+\mu_i m_b)/2$ indeed satisfies the condition. If we decompose the Hamiltonian into the contribution of the stochastic field and the rest as

$$\mathcal{H}_\mu = \mathcal{H}_0 - J\sum_i \mu_i\sigma_i, \tag{2.2}$$

where

$$\mathcal{H}_0 := -J\sum_{i<j}\sigma_i\sigma_j - h^{\mathrm{ext}}\sum_i \sigma_i, \tag{2.3}$$

the partition function of the system is written in the form

$$\mathcal{Z} = \left\langle \mathrm{Tr}_\sigma \left[\mathrm{e}^{-\beta \mathcal{H}_\mu} \right] \right\rangle_\mu = \mathrm{Tr}_\sigma \left[\mathrm{e}^{-\beta \mathcal{H}_0} \left\langle \prod_i \mathrm{e}^{\beta J \mu_i \sigma_i} \right\rangle_\mu \right] \tag{2.4}$$

$$= (\cosh \beta J)^N \ \mathrm{Tr}_\sigma \left[\mathrm{e}^{-\beta \mathcal{H}_0} \prod_j (1 + \sigma_i m_\mathrm{b} \tanh \beta J) \right]. \tag{2.5}$$

Let us assume that the boundary magnetization of one sliding surface acts as an effective field h_b on the boundary magnetization of the other. The model then reduces to

$$\mathcal{H}_\mathrm{eq} := -J \sum_{i<j} \sigma_i \sigma_j - h_\mathrm{b} \sum_i \sigma_i = \mathcal{H}_0 - b \sum_i \sigma_i, \tag{2.6}$$

with $b := h_\mathrm{b} - h^\mathrm{ext}$, which relaxes toward the equilibrium state. Its partition function is written as

$$\mathcal{Z}_\mathrm{eq}(\beta, b) = \mathrm{Tr}_\sigma \left[\mathrm{e}^{-\beta \mathcal{H}_\mathrm{eq}} \right] = \mathrm{Tr}_\sigma \left[\mathrm{e}^{-\beta \mathcal{H}_0} \sum_i \mathrm{e}^{\beta b \sigma_i} \right] \tag{2.7}$$

$$= \prod_i \cosh \beta b \ \mathrm{Tr}_\sigma \left[\mathrm{e}^{-\beta \mathcal{H}_0} \prod_i (1 + \sigma_i \tanh \beta b) \right]. \tag{2.8}$$

Comparing the right-hand sides of Eqs. (2.5) and (2.8), we have $\mathcal{Z} \propto \mathcal{Z}_\mathrm{eq}$ if it holds that $\tanh \beta b = m_\mathrm{b} \tanh \beta J$. By this relation we can regard our non-equilibrium model as another equilibrium model with an additional boundary magnetic field. We thus have

$$h_\mathrm{b} = \tanh^{-1} (m_\mathrm{b} \tanh K) \tag{2.9}$$

in the limit $h^\mathrm{ext} \to 0$. The boundary magnetization under a static field h_b has a form of

$$m_{\mathrm{b,eq}}(\beta, h_\mathrm{b}) := \frac{\partial}{\partial h_\mathrm{b}} \log \mathcal{Z}_\mathrm{eq}(\beta, h_\mathrm{b}), \tag{2.10}$$

and thus we have

$$m_{\mathrm{b,eq}} \left(\beta, \tanh^{-1} (m_b \tanh K) \right) = m_\mathrm{b} \tag{2.11}$$

as a self-consistent relation for m_b.

The critical point is given by

$$1 = \frac{\partial}{\partial m_\mathrm{b}} m_{\mathrm{b,eq}}(\beta, \tanh^{-1} (m_b \tanh K)) \Big|_{m_\mathrm{b}=0}. \tag{2.12}$$

Expanding the left-hand side of Eq. (2.11) to the first order of m_b and using the condition (2.12), we have

$$m_{\mathrm{b,eq}} (\beta, 0) + m_b \tanh (\beta J) \left. \frac{\partial m_{\mathrm{b,eq}}(\beta, h_\mathrm{b})}{\partial h_\mathrm{b}} \right|_{h_\mathrm{b}=0} = m_\mathrm{b}. \tag{2.13}$$

With the definition of the equilibrium boundary susceptibility

$$\chi_{\mathrm{b,eq}}(\beta) := \left.\frac{\partial m_{\mathrm{b,eq}}(\beta, h_{\mathrm{b}})}{\partial h_{\mathrm{b}}}\right|_{h_{\mathrm{b}}=0} \tag{2.14}$$

and the fact $m_{\mathrm{b,eq}}(K, 0) = 0$, we finally have

$$\tanh(\beta)\, \chi_{\mathrm{b,eq}}(\beta) = 1. \tag{2.15}$$

The condition (2.15) determines the non-equilibrium critical temperature $\beta = \beta_{\mathrm{c}}$. Using the exact expressions of the magnetization for the one-dimensional Ising model and the boundary magnetization for the two-dimensional model, we have the solutions of the condition (2.15) as

$$\beta_{\mathrm{c}} J^{-1} = \frac{k_{\mathrm{B}} T}{J} = \begin{cases} 2.2691853\ldots & \text{in one dimension,} \\ 2.6614725\ldots & \text{in two dimensions.} \end{cases} \tag{2.16}$$

The latter corresponds to $T_{\mathrm{c}}^{*}(\infty)$ in Fig. 2.2. The former, on the other hand, has the same value as in the two-dimensional *equilibrium* Ising model. The equilibrium boundary susceptibility of the one-dimensional Ising model is given by

$$\chi_{\mathrm{b,eq}}(\beta) = \mathrm{e}^{2\beta J}, \tag{2.17}$$

which reduces Eq. (2.15) to the relation

$$\tanh(\beta)\, \mathrm{e}^{2\beta J} = 1. \tag{2.18}$$

This gives the two-dimensional equilibrium critical point, accidentally as far as we understand. The non-equilibrium critical temperature in the two-dimensional model is higher than that in the one-dimensional one, because in general the effect of the mean field is stronger for higher dimensions under the same perturbation.

Chapter 3

Numerical Simulations

In this chapter, we present the way of calculating the frictional force as a non-equilibrium physical quantity. This method for lattice spin systems was first introduced by Kadau *et al.* [21] and has widely used in related works until now [1, 23, 25–28]. We also explain, in particular, the convergence to the non-equilibrium steady state by our Monte Carlo simulation method.

3.1 Setup of the Model

Sliding friction is a form of energy dissipation on the surface between a moving object and its substrate. The dissipated energy is originated in the kinetic energy of the moving object. We here consider a constantly moving case in which an external force maintains the motion of the object with endless supply of its kinetic energy. This view leads to its *non-equilibrium stationary state* (see Fig. 3.1). We will show in Fig. 3.4 below our simulation data of the energy changes.

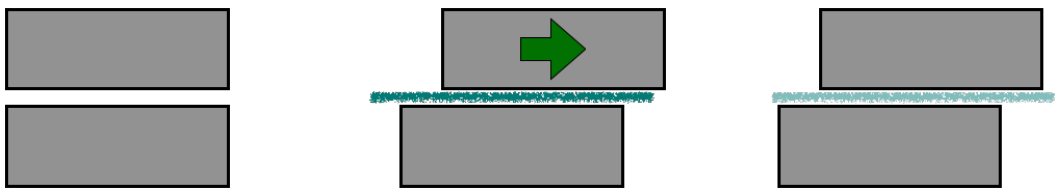

(a) (b) (c)

Figure 3.1: Schematic picture of a moving object and a substrate. If the whole system is in the equilibrium state (a), the motion of the upper object makes a change of the boundary energy, which has a positive value in the ensemble average (b). Interacting with the surrounding environment, the system tries to relax to the equilibrium state again (c). The perpetual motion by an external force, however, prevents the system from going back to the equilibrium state; instead the system goes to the non-equilibrium stationary state.

When the system is in a non-equilibrium stationary state, it is often easy to calculate *energy currents* such as the frictional heat, its power and so on. Applying the view to our case in which two square lattices of the Ising model slide against each other, we can formulate the problem as follows; see Fig. 3.2.

1. We prepare a square lattice of the Ising model of size $L_x \times L_z$ and impose periodic boundary conditions in the transverse (x) direction, whereas we set the open boundary conditions in the longitudinal (z) direction for the moment. We first set the system in the equilibrium state of a temperature T.

2. We cut the system along the x-direction into two parts, maintaining interactions on the cut.

3. We slide two parts along the cut plane with relative velocity v. In other words, we shift the upper half by a lattice constant every $1/v$ unit time.

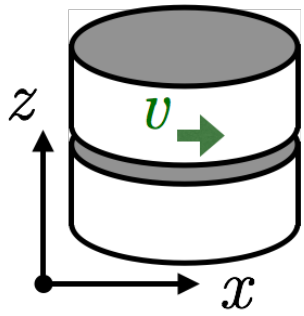

Figure 3.2: Two cylinders of the Ising model sliding with the velocity v.

The Hamiltonian of the system is given by

$$H = H_{\text{upper}} + H_{\text{lower}} + H_{\text{slip}}(t), \tag{3.1}$$

where

$$H_{\text{upper}} := -J \sum_{\langle i,j \rangle \in \text{upper}} \sigma_i \sigma_j, \tag{3.2}$$

$$H_{\text{lower}} := -J \sum_{\langle i,j \rangle \in \text{lower}} \sigma_i \sigma_j, \tag{3.3}$$

$$H_{\text{slip}}(t) := -J \sum_{\langle i,j(t) \rangle \in \text{slip}} \sigma_i \sigma_{j(t)} \tag{3.4}$$

with the subscripts upper, lower and slip representing the set of neighboring spin pairs on the upper half, the lower half and the slip plane, respectively. In $H_{\text{slip}}(t)$, the ith spin on the boundary above the cut changes the opponent of the interaction on the boundary below the cut as indicated by $j(t)$ when the upper lattice shifts against the lower one. We alternate the shift operations and the Monte Carlo spin flips in our simulation. We will give the details of the simulation schedule below in Sec. 3.2.2.

Shift operations on the upper lattice lead the system to repeated *pumping* and *dissipation* processes as follows:

1. **Shift**: A shift operation excites the energy on the slip plane by the amount $\langle H_{\text{slip}}(t') - H_{\text{slip}}(t) \rangle_{\text{st}}$, where the letter t' denotes the time just after the shift operation at time t.

2. **Relax 1**: The excited energy on the slip plane $\langle H_{\rm slip}(t') - H_{\rm slip}(t)\rangle_{\rm st}$ dissipates to the entire system.

3. **Relax 2**: The excited entire system relaxes towards the equilibrium.

Our model always reaches a non-equilibrium stationary states in the long-time limit $t \to \infty$, which depends on the temperature T and the sliding velocity v; see Sec. 3.2.3 for the proof. We define the stationary-state average $\langle A\rangle_{\rm st} := \sum_i A_i p_i^{\rm (st)}$ for an arbitrary observable A, where $\{A_i\}$ are observed values of A and $p_i^{\rm (st)}$ denotes the stationary-state probability distribution, which is different from the equilibrium (canonical) probability distribution $p_i^{\rm (eq)} \propto \exp\left[-E_i/(k_{\rm B}T)\right]$.

3.2 Non-equilibrium Monte Carlo Simulation

The dissipation process towards the heat bath occurs via a spin flip. This fundamental processes do not only describe the equilibrium state but also the non-equilibrium stationary state at a fixed temperature parameter T [31]. Using the Monte Carlo method, we simulate this process.

3.2.1 Introduction of the Time Scale to Ising Models

In order to calculate dynamical observables such as the frictional power (3.7) and its dissipation rate (3.8), we have to define *a unit time* for the simulation of the finite-size system.

For the equilibrium Monte Carlo simulation, the most naive approach for the equilibrium state is the single-spin-flip algorithm, where we perform the sequence of a random selection of a spin and its flip with a temperature-dependent probability $p(T)$. We use the probability that satisfies the *detailed balance condition*, which certainly leads the system towards the true equilibrium state with enough repetition of the sequence. For example, we often use the Metropolis probability $p_{\rm M}(T) := \min\{1, \exp\left[-\Delta E/(k_{\rm B}T)\right]\}$ as the probability $p(T)$, where ΔE is the energy difference due to the flip. We often call a *Monte Carlo step* a single process of the algorithm, and define a *Monte Carlo sweep* by N Monte Carlo steps, where N is the number of spins.

Which should we use as a unit time, a Monte Carlo step or a Monte Carlo sweep? Its answer can be found in the following manner. We usually assume that a statistical mechanical system is coupled to a heat bath by every local degree of freedom. The temperature of the system is kept constant by the heat bath, and the system exchanges its energy with the heat bath through local degrees of freedom. It is most symmetric to assume that the equilibrium relaxation of a macroscopic system takes place in the same time scale if the volume of the system is doubled. Thus the number of times of the energy exchanges is proportional to the total number of degrees of freedom of the system. This justifies to define a unit time by a Monte Carlo sweep; the relaxation time would be proportional to the total number of degrees of freedom if we used the Monte Carlo steps for a unit time.

3.2.2 Slip Plane with the Velocity v

Using the introduced time scale, we can also introduce the sliding velocity v of the system with N spins, where $N = L_x \times L_z$. Corresponding to the setup in Sec. 3.1, we perform an extended single-spin-flip algorithm with the following unit Monte Carlo time:

1. **Shift**: We shift the upper half of the lattice by a lattice constant.

2. **Flip**: We perform ordinary single flips for (N/v) times, which is the $(1/v)$ fraction of a Monte Carlo sweep.

3. We repeat the processes 1 and 2 for v times.

In the extended algorithm, the upper half slides with the velocity v in a unit time at regular intervals. The frictional power $P(t)$ and the dissipation rate $D(t)$ are measured in Monte Carlo simulations as the energy differences for a unit time due to the shift and the flip operation, respectively (see Section 3.3 for definitions of the frictional power $P(t)$ and the dissipation rate $D(t)$).

Magnetic frictions in the Ising model are described by the following elementary process. Suppose that the system is in an equilibrium state with a snapshot as in Fig. 3.3(a). A sliding operation stretches the domain wall across the sliding boundary as in Fig. 3.3(b). The stretched domain wall tends to shrink by thermal fluctuations as in Fig. 3.3(c). The energy of the system jumps at the stretching process and decays at the shrinking process. The sums of these energy changes for a Monte Carlo sweep are equal to our observed quantities $P(t)$ and $D(t)$, respectively.

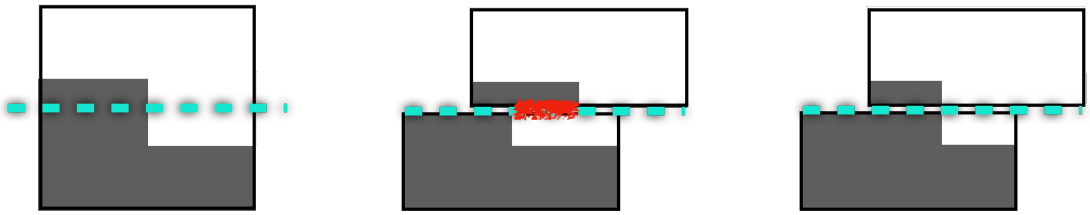

(a) (b) (c)

Figure 3.3: A schematic picture of magnetic frictions in an elementary process.

We show an example of the time series of the bulk energy (see Fig. 3.4). We thermalized the system of size 20×20 for 40,000 MC steps and equilibrated it at the temperature $T = 2.50$. We then make the system slide with the constant velocity $v = 1$ from the time $t = 40{,}001$ MC step for 40,000 MC steps until the time $t = 80{,}000$ MC step. The energy takes the value of the equilibrium state just after the start point of sliding (see Fig. 3.4(a)). After a sufficient length of the time, however, the average value of the energy converges to a new value of the non-equilibrium stationary state (see Fig. 3.4(b)). For each 400 MC steps, which corresponds to a MC sweep, a sliding operation makes the energy *jump* and the relaxation process by spin flips make it *decay*. The sum of contributions to the energy by jump and decay processes for a MC sweep are equal to the value of $P(t)$ and $D(t)$, respectively. Both the frictional power $P(t)$ and the dissipation rate $D(t)$ have the same absolute value in the long-time limit.

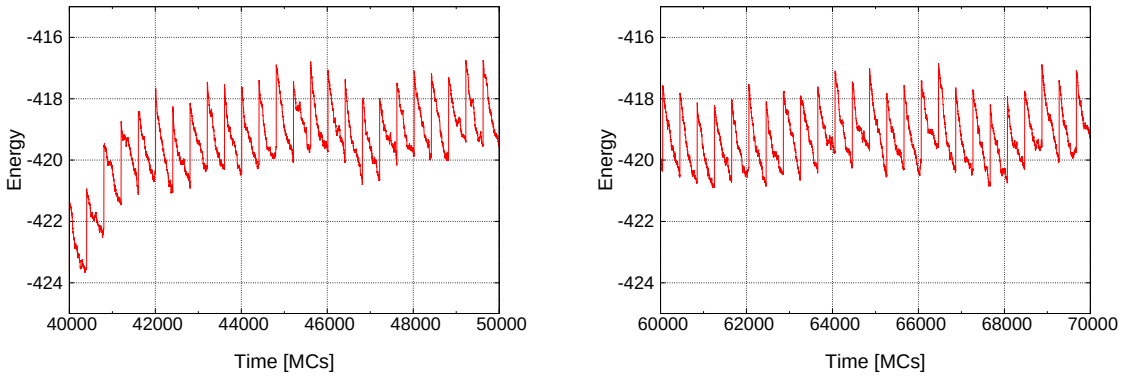

(a) (b)

Figure 3.4: Time series of the energy of the whole system in regimes of non-equilibrium relaxation from the equilibrium state (a) and in the non-equilibrium stationary state (b).

A comment on our algorithm is in order. The shift operation and spin flips occur in one Monte Carlo sweep but separately, which may or may not reproduce the real situation of relaxation while sliding. A possible alternative is to introduce a distance-dependent exchange interaction between the spins above and below the cut and change the interaction continuously in time. Here we choose to stick to our algorithm for simplicity.

3.2.3 Convergence to the Non-equilibrium Stationary State

The convergence to a unique non-equilibrium stationary state is ensured in the following way. The above algorithm is represented by the following matrix for a Monte Carlo sweep:

$$\hat{T}(\beta, v) := \left[\left(\hat{M}(\beta) \right)^{N/v} \hat{S} \right]^{v}, \tag{3.5}$$

where $v \in \{\text{Divisors of } N\}$. The matrix $\hat{M}(\beta)$ and $\hat{S}$ express a Monte Carlo step at a temperature T and sliding of the upper half by a lattice constant, respectively, for the model of size $N = L_x \times L_z$. The matrix $\hat{T}(\beta, v)$ describes the time evolution for a Monte Carlo sweep, because the matrix have the Nth power of $\hat{M}(\beta)$. The matrices $\hat{M}(\beta)$ and $\hat{S}$ belong to the class called the *stochastic matrix*, which is defined by the following properties:

- Each element is greater than or equal to zero;
- Each row-wise total sum of elements is normalized to unity.

The product of two stochastic matrices is also a stochastic matrix. Indeed if we have two Ω-dimensional stochastic matrices $\hat{A}$ and $\hat{B}$, we have

$$\sum_{i=1}^{\Omega} (\hat{A}\hat{B})_{ij} = \sum_{i=1}^{\Omega} \sum_{k=1}^{\Omega} A_{ik} B_{kj} = \sum_{k=1}^{\Omega} \left(\sum_{i=1}^{\Omega} A_{ik} \right) B_{kj} = \sum_{k=1}^{\Omega} B_{kj} = 1 \quad \text{for } 1 \leq j \leq \Omega, \tag{3.6}$$

and therefore the matrix $\left(\hat{M}(\beta)\right)^{N/v}\hat{S}$ is also a stochastic matrix. Any stochastic matrix has at least the eigenvalue 1 (see App. A), and therefore the matrix $\left(\hat{M}(\beta)\right)^{N/v}\hat{S}$ also has the eigenvalue 1.

We now use the concept of *strong connectivity* of stochastic matrices, which ensures that the the eigenvalue 1 is the only eigenvalue of absolute value 1 and the moduli of all other eigenvalues are less than 1. If a stochastic matrix $\hat{A}$ satisfies the condition that any element of the power $\left(\hat{A}\right)^{N_0}$ is positive for an integer N_0, we call the matrix $\hat{A}$ strongly connected. Namely, we can say that if the matrix $\hat{T}(\beta, v)$ is strongly connected the corresponding simulation always converges to the non-equilibrium stationary state.

We first show that the matrix $\left(\hat{M}(\beta)\right)^{N}$ is a strongly connected stochastic matrix. If we consider an N-spin Ising system, a transition from a state i to a state j can be obviously achieved by at most N times of single-spin flip (**SSF**). If we need $n(i,j)$ times of SSF for the process, we have only to stay at the state j for $N - n(i,j)$ times in order to achieve the process by exactly N times of SSF. In the Metropolis algorithm, we can stay at any state with the exception of the highest-energy state, where the acceptance rate of any SSF are equal to unity. For the Glauber algorithm, we can stay at any state because of the probability $p_{\mathrm{G}}(T) := (\mathrm{e}^{\Delta E_{ij}/k_{\mathrm{B}}T} + 1)^{-1}$, where the rejection rate of an SSF is always nonzero. Thus we can make a path between an arbitrary pair of states (i,j) by exactly N times of SSF. In other words, we can construct a product $M_{i,k_1}M_{k_1,k_2}M_{k_2,k_3}\dots M_{k_{N-1},k_N} > 0$ ($k_N = j$), where $M_{i,j}$ is an element of the ith column and the jth row of the matrix $\hat{M}(\beta)$. We therefore conclude that the matrix $\left(\hat{M}(\beta)\right)^{N}$ is a strongly connected stochastic matrix.

We next show that the matrix $\hat{T}(\beta, v)$ is also strongly connected. We can regard the matrix $\hat{T}(\beta, v)$ as a decomposition of the product $\left(\hat{M}(\beta)\right)^{N}$ into v equivalent pieces. To make a transition from a state j to a state j, we only have to perform SSFs at each Nn/v steps ($n = 1, 2, \dots, v$) so that the final state may be equal to j, with only differences by the product $\left(\hat{S}\right)^{v-n+1}$. Such a nonzero amplitude $\left(\left[\left(\hat{M}(\beta)\right)^{N/v}\hat{S}\right]^{v}\right)_{i,j}$ can be achieved for an arbitrary pair of states (i,j) by analogy with the case of $\left(\hat{M}(\beta)\right)^{N}$. We thus conclude that the matrix $\hat{T}(\beta, v)$ is a strongly connected stochastic matrix, and that the matrix $\hat{T}(\beta, v)$ is a positive stochastic matrix, which implies that our simulation always converges to a unique non-equilibrium stationary state.

3.2.4 Concrete examples of matrices $\hat{M}(\beta)$ and $\hat{S}$

The matrices $\hat{M}(\beta)$ and $\hat{S}$ have sparse structures as demonstrated in Figs. 3.5(a) and (b), respectively, whereas the matrix $\hat{T}(\beta, v)$ has a dense structure as in Fig. 3.5(c). The task of diagonalizing the matrix $\hat{T}(\beta, v)$ is the same as that of $\left(\hat{M}(\beta)\right)^{N/v}\hat{S}$, which corresponds to the time evolution for the $(1/v)$ fraction of a Monte Carlo sweep. We show in Fig. 3.6 the eigenvalue distributions of $\left(\hat{M}(\beta)\right)^{N/v}$ and $\left(\hat{M}(\beta)\right)^{N/v}\hat{S}$ for the model of

size $L_x = 3, L_z = 2$. These eigenvalue distributions are somewhat similar to each other, which reflects the fact that both of them correspond to the time evolution for the same time.

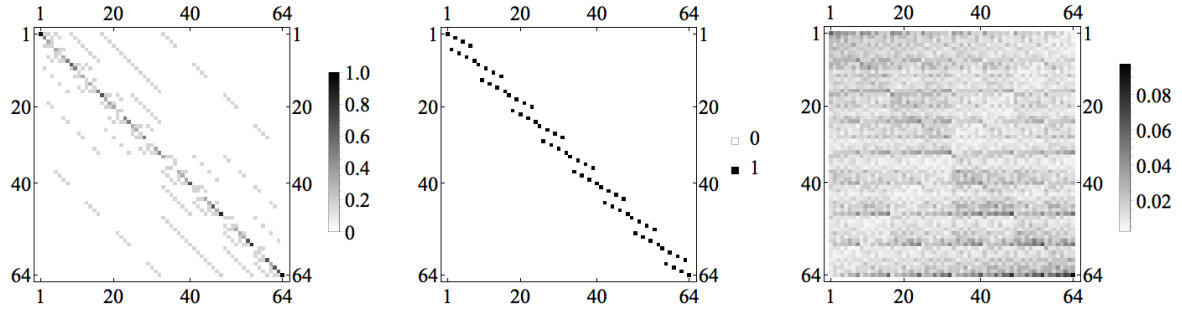

(a) (b) (c)

Figure 3.5: The array plots of matrices for the model of size $L_x = 3, L_z = 2$ and at the temperature $T = 10$: (a) $\hat{M}(\beta)$; (b) $\hat{S}$; (c) $\hat{T}(\beta, v)$.

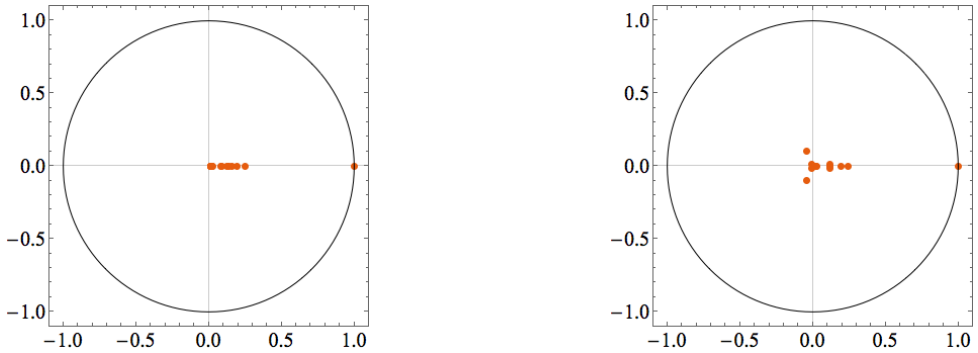

(a) (b)

Figure 3.6: Eigenvalue distributions of matrices for the model of size $L_x = 3, L_z = 2$ and at the temperature $T = 10$: (a) $\left\{\hat{M}(\beta)\right\}^{N/v}$; (b) $\left\{\hat{M}(\beta)\right\}^{N/v} \hat{S}$.

3.3 Definitions of Physical Quantities

The excited and relaxed amounts of energy per unit time correspond to the energy pumping and dissipation, respectively. The energy pumping $P(t)$ and the energy dissipation $D(t)$ are given by

$$P(t) := \sum_{i_v=0}^{v-1} \left[H_{\text{slip}}\left(t' - 1 + \frac{i_v}{v}\right) - H_{\text{slip}}\left(t - 1 + \frac{i_v}{v}\right) \right], \tag{3.7}$$

$$D(t) := \sum_{i_v=0}^{v-1} \left[H\left(t - 1 + \frac{i_v + 1}{v}\right) - H\left(t' - 1 + \frac{i_v}{v}\right) \right], \tag{3.8}$$

respectively. They correspond to the energy differences due to the **Shift** and the **Relax** processes. Note that we obtain the former and the latter for the slip plane and the entire system, respectively, and that the absolute values of $P(t)$ and $D(t)$ become equal to each other in the non-equilibrium stationary state.

We now consider the case in which the system is in a non-equilibrium stationary state. We denote by $P(L_x, L_z, T)$ and $D(L_x, L_z, T)$ the long-time limit of the energy pumping $P(t)$ and the energy dissipation $D(t)$, respectively, for a system of size $L_x \times L_z$ at the temperature T: $P(L_x, L_z, T) = \langle P(t) \rangle_{\rm st}$, $D(L_x, L_z, T) = \langle D(t) \rangle_{\rm st}$. We define the frictional force density $f(L_z, T)$ by

$$f(L_z, T) := \lim_{L_x \to \infty} \frac{F(L_x, L_z, T)}{L_x}, \tag{3.9}$$

where $F(L_x, L_z, T)$ is the long-time limit of the frictional force. We can calculate the frictional force $F(L_x, L_z, T)$ using its power $D(L_x, L_z, T)$ by the formula

$$F(L_x, L_z, T) = \frac{D(L_x, L_z, T)}{v}, \tag{3.10}$$

because the energy to dissipate in unit time is injected as the work done by the frictional force in unit time.

We use the fact that $\lim_{t\to\infty} |D(t)| = \lim_{t\to\infty} |P(t)|$ in order to estimate $D(t)$ because the Monte Carlo estimate of $P(t)$ has less statistical fluctuation [23, 29, 30]. In the long-time limit, we therefore have

$$f(L_x, L_z, T) = \lim_{L_x \to \infty} \frac{P(L_x, L_z, T)}{v L_x}. \tag{3.11}$$

We also define the bulk energy density $\epsilon(L_z, T)$ as follows:

$$\epsilon(L_z, T) := \lim_{L_x \to \infty} \frac{E_{\rm b}(L_x, L_z, T)}{L_x L_z}, \tag{3.12}$$

where $E(L_x, L_z, T)$ is the energy of the entire system. From this, we define the bulk heat capacity $c(L_z, T)$ as follows:

$$c(L_z, T) := \frac{\partial \epsilon(L_z, T)}{\partial T}. \tag{3.13}$$

Chapter 4

Results

In this chapter, we first show in Sec. 4.1 our numerical results of the frictional force density $f(L_z, T)$, the bulk energy density $\epsilon(L_z, T)$ and their temperature derivatives. We also show in Sec. 4.2 that the numerical infinite-size limit $L_x \to \infty$ converges with L_z and T fixed.

The range of parameters in our simulation is as follows. We computed the value of $f(L_z, T)$ for temperatures $k_{\rm B}T/J \in \{0.0, 0.1, 0.2, \ldots, 1.9, 2.0, 2.02, 2.04, \ldots, 2.48, 2.50, 2.6, 2.7, \ldots, 5.0\}$ and sizes $L_z \in \{4, 8, 16, 32, 64\}$ with the anti-parallel and the parallel boundary conditions. For the anti-parallel boundary conditions, we set the initial state to the domain-wall state, where spin variables σ_i in the upper half of the system have the same value as the spins on the upper boundary and those in the lower half as the spins on the lower boundary. For the parallel boundary conditions we set the initial state to the magnetized state, where all spin variables σ_i have the same value as both of boundaries. The reason why we used these initial states is that they are the most symmetric ground states which correspond to each set of boundary conditions.

All the simulations are performed by the single-flip algorithm with the Metropolis rate at the temperature T. To obtain the observables in the non-equilibrium stationary state, we performed the equilibration process for 5,000 sweeps without shift operations and the stationarization process for 5,000 sweeps for all given parameters. We checked the convergence of the observables to the equilibrium values and the stationary values for these time regions by fitting the observables to the function $A(t) = A_0 + A_1 \mathrm{e}^{-t/\tau}$. The duration of 5,000 sweeps is substantially longer than the fitting parameter τ, which we call the *non-equilibrium relaxation time*. We performed these simulations for 480 samples for all parameters and averaged them, and then averaged along the time direction. The statistical errors of the data presented in the present chapter are all smaller than the point size.

4.1 Observed Quantities

4.1.1 Frictional Force Density $f(L_z, T)$

We show the behavior of the frictional force density $f(L_z, T)$ in Fig. 4.1. The results of $f(L_z, T)$ for both boundary conditions converge to almost the same results for the size $L_z = 64$; compare the blue curves in Fig. 4.1(a) and (b). We thereby decide that the

size $L_z = 64$ is a good approximation for the limit of $L_z \to \infty$. This behaves similarly to the result in Ref. [21] although for different parameters. Towards this limit, $f(L_z, T)$ increases for the anti-parallel boundary conditions, whereas $f(L_z, T)$ decreases for the parallel boundary.

When the size L_z is larger than the correlation length $\xi_z(\beta)$ along the z direction perpendicular to the cut, the system behaves as a two-dimensional one and the effects of the boundary conditions vanish, whereas when the size L_z is smaller than $\xi_z(\beta)$ the system is effectively one-dimensional. We can consider this behavior as a dimensional crossover.

4.1.2 Bulk Energy Density $\epsilon(L_z, T)$

We show the behavior of the bulk energy density $\epsilon(L_z, T)$ in Fig. 4.2. As the frictional force density $f(L_z, T)$, the bulk energy density $\epsilon(L_z, T)$ also indicates asymptotic behavior in the limit of $L_z \to \infty$ as well as difference due to the boundary conditions for small L_z, reflecting the dimensional crossover.

4.1.3 Temperature Derivatives $\partial f(L_z, T)/\partial T$ and $c(L_z, T)$

We additionally show the behavior of temperature derivatives $\partial f(L_z, T)/\partial T$ and $c(L_z, T) = \partial \epsilon(L_z, T)/\partial T$ in Figs. 4.3 and 4.4, respectively. They exhibit sharp peaks at a characteristic temperature $k_{\mathrm{B}}T/J = 2.40$ (see the red vertical line in Fig. 4.3) and $k_{\mathrm{B}}T/J = 2.27$ (see the black vertical line in Fig. 4.4), respectively, for both boundary conditions for the largest size $L_z = 64$. This implies that they diverge in the limit of $L_z \to \infty$. We observe that the finite-size peak $k_{\mathrm{B}}T_{\mathrm{peak}}(L_z)/J$ shifts to lower temperatures for the anti-parallel boundary conditions and to higher temperatures for the parallel boundary conditions. This observation shows us that the anti-parallel boundary conditions generate a *disordering* effect, while the parallel boundary conditions generate an *ordering* effect. These effects are most enhanced for small L_z.

The peak locations $k_{\mathrm{B}}T/J = 2.40$ and $k_{\mathrm{B}}T/J = 2.27$ show good agreements with the non-equilibrium phase transition point $T_{\mathrm{c}}^{\mathrm{M}}(v)$ with the velocity $v = 10$ in Ref. [1] and the bulk phase transition point, respectively; see Fig. 4.5. We can regard both divergent behaviors as intrinsic phase transitions independent of the boundary conditions, because the effect of boundary conditions vanishes in the limit of $L_z \to \infty$.

We also consider the reason why not only the heat capacity $c(L_z, T)$ but also the temperature derivative of the frictional force density $\partial f(L_z, T)/\partial T$ shows the divergent behavior. The frictional force density $f(L_z, T)$ is estimated by the difference between the expectation value of the energy before and after the sliding. It is therefore plausible that both expectation values have a singularity near $k_{\mathrm{B}}T/J = 2.40$, and these singularities do not cancel with each other.

4.2 Checking the Convergence in the Limit $L_x \to \infty$

We now demonstrate that the following two observables converge in the infinite-size limit $L_x \to \infty$:

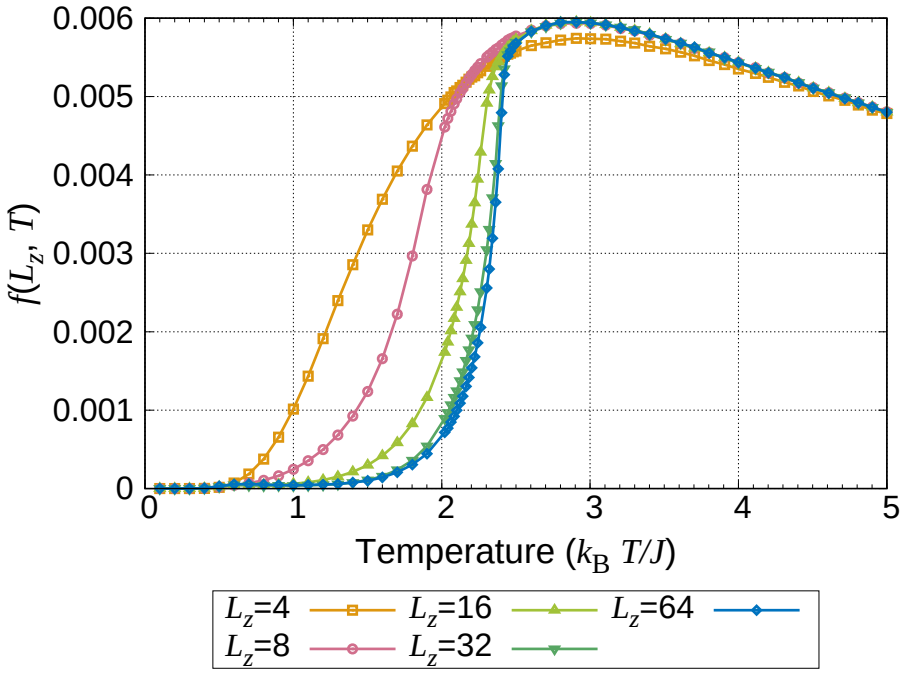

(a)

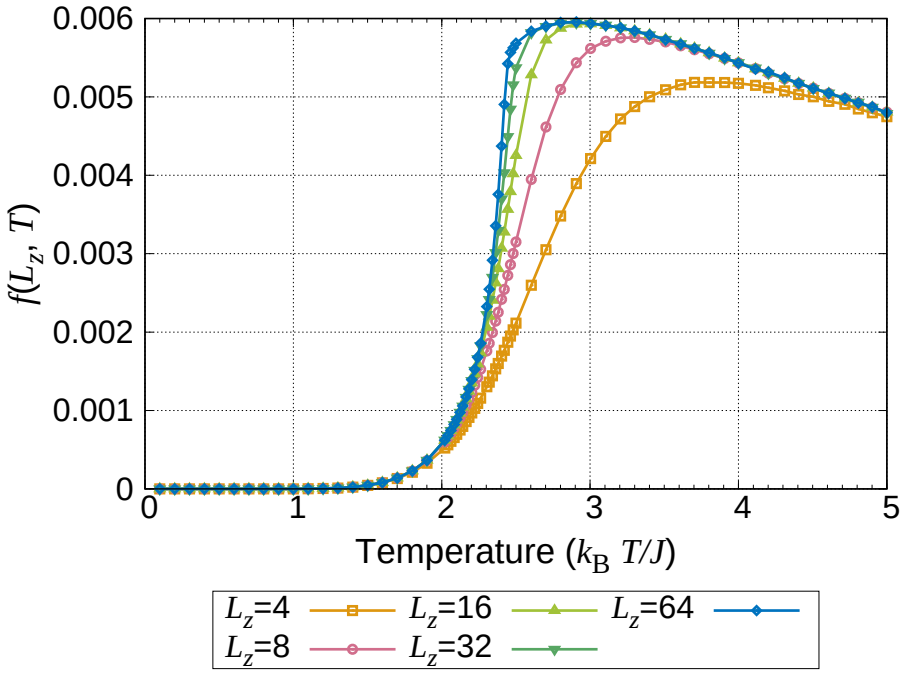

(b)

Figure 4.1: Temperature dependence of $f(L_z, T)$ with each boundary condition: (a) The anti-parallel boundary conditions; (b) The parallel boundary conditions.

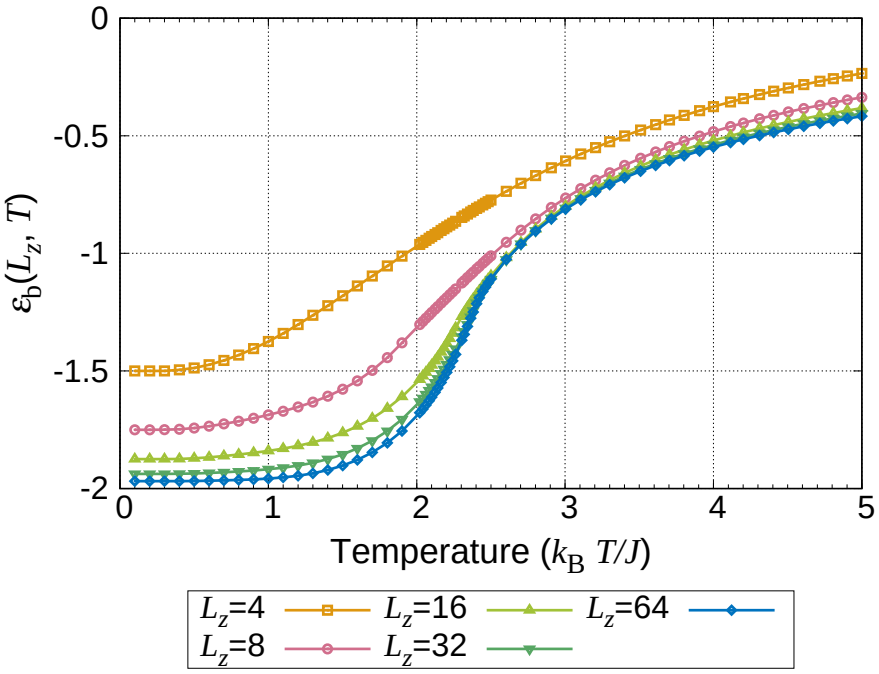

(a)

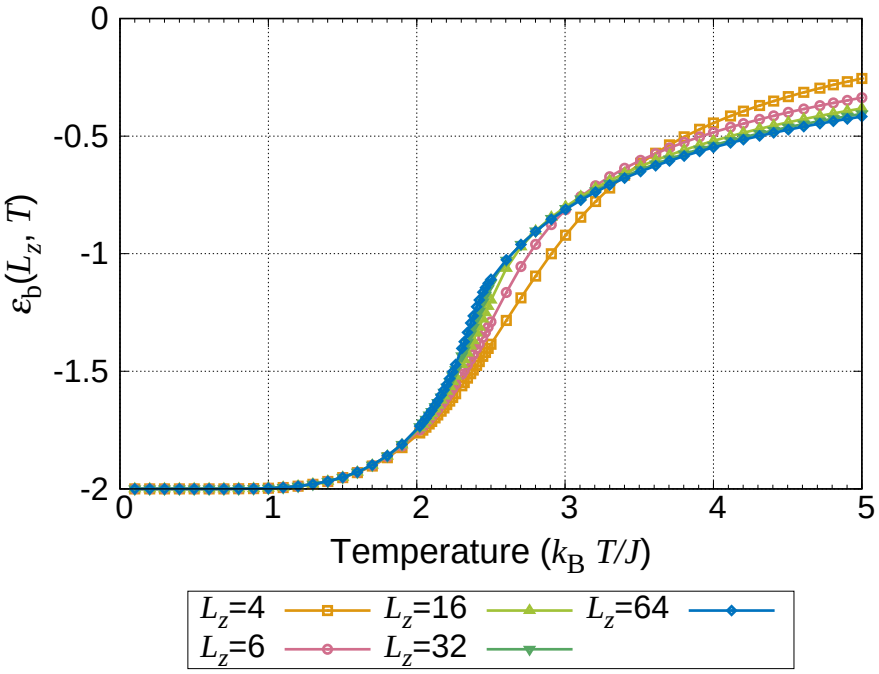

(b)

Figure 4.2: Temperature dependences of $\epsilon(L_z, T)$ with each boundary condition: (a) The anti-parallel boundary conditions; (b) The parallel boundary conditions.

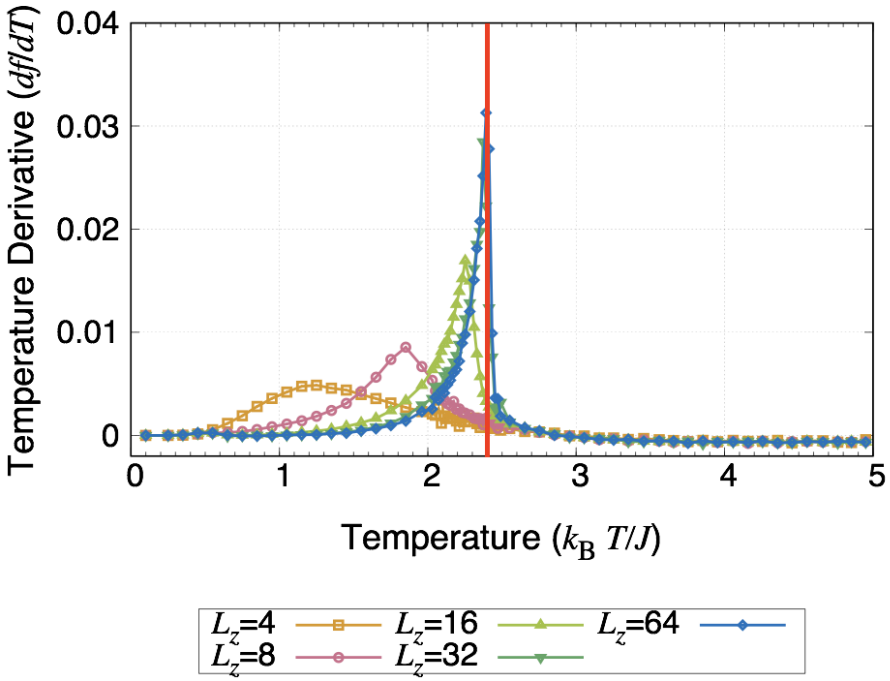

(a)

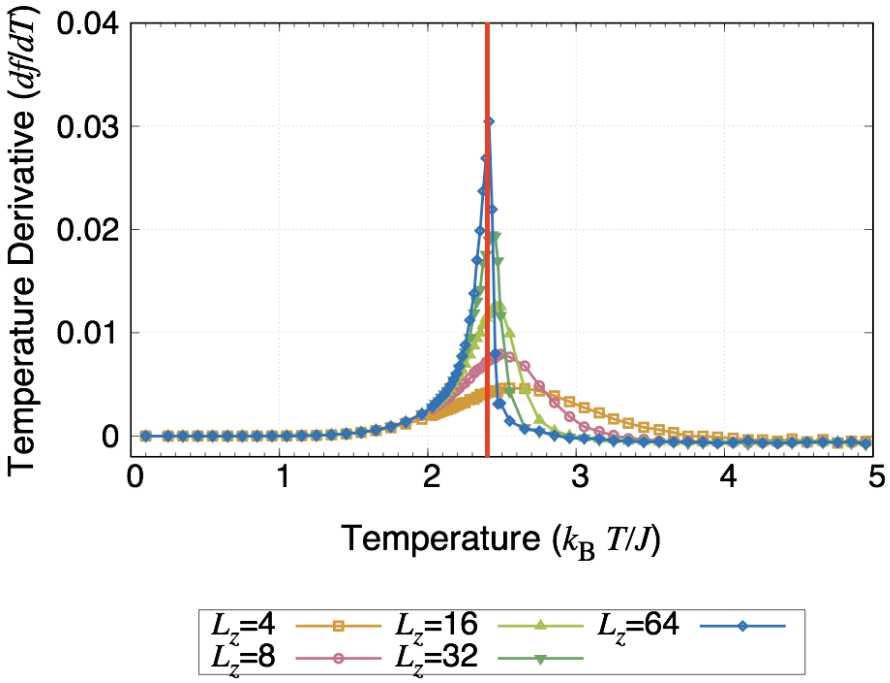

(b)

Figure 4.3: Temperature dependence of $\partial f(L_z, T)/\partial T$ with each boundary condition: (a) The anti-parallel boundary conditions; (b) The parallel boundary conditions. The vertical red line in each panel indicates the non-equilibrium critical temperature $T_c^{\mathrm{M}}(10) \simeq 2.40$, where we choose the unit $k_{\mathrm{B}}/J = 1$, in the phase diagram of the two-dimensional non-equilibrium Ising model obtained in Ref. [1]; see Fig. 4.5.

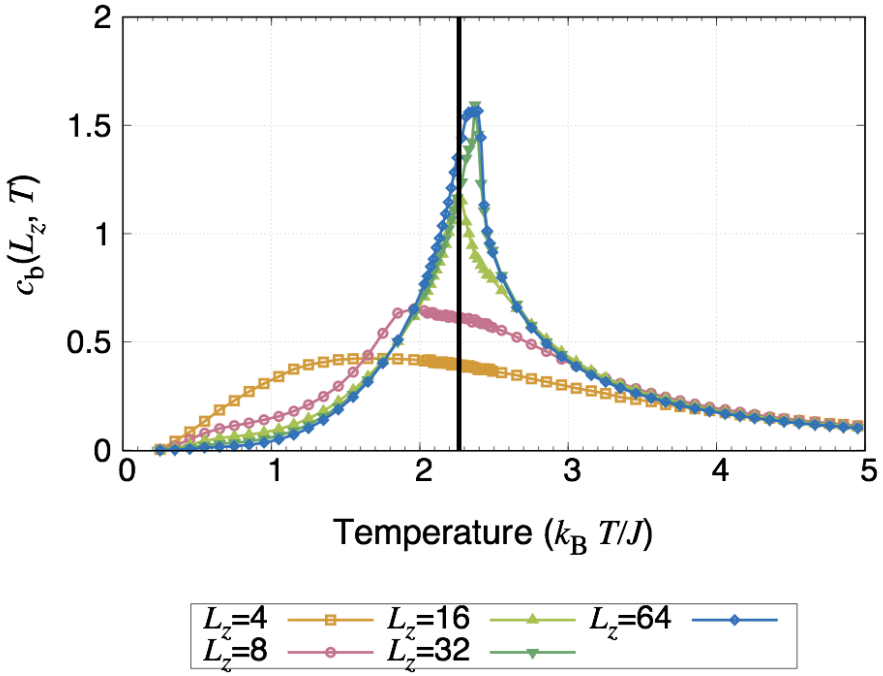

(a)

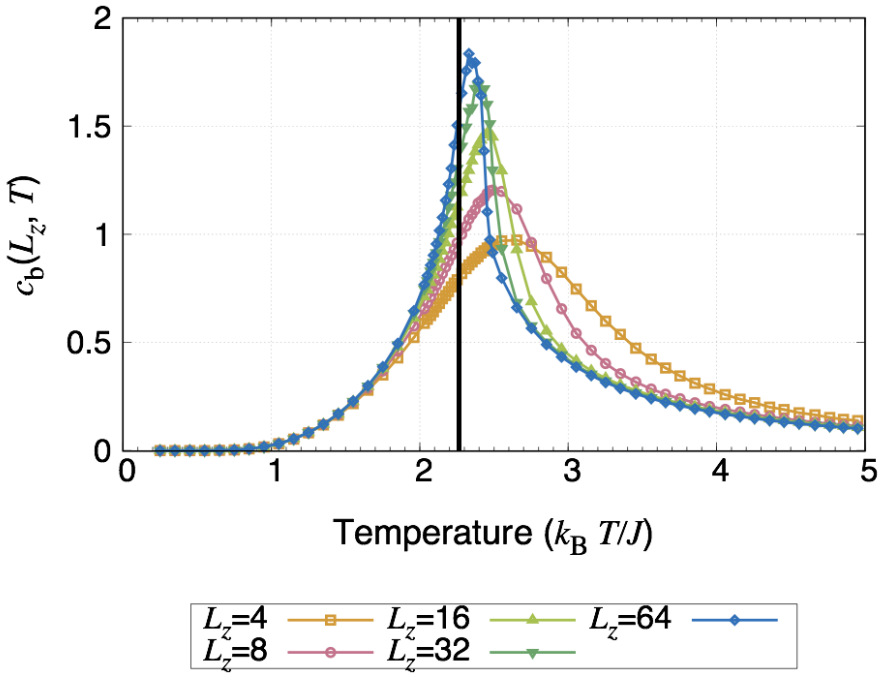

(b)

Figure 4.4: Temperature dependences of $c(L_z, T) = \partial\epsilon(L_z, T)/\partial T$ with each boundary condition: (a) The anti-parallel boundary conditions; (b) The parallel boundary conditions. The vertical black line in each panel indicates the equilibrium critical temperature $T_{\mathrm{c,eq}} \simeq 2.27$, where we choose the unit $k_{\mathrm{B}}/J = 1$; see Fig. 4.5.

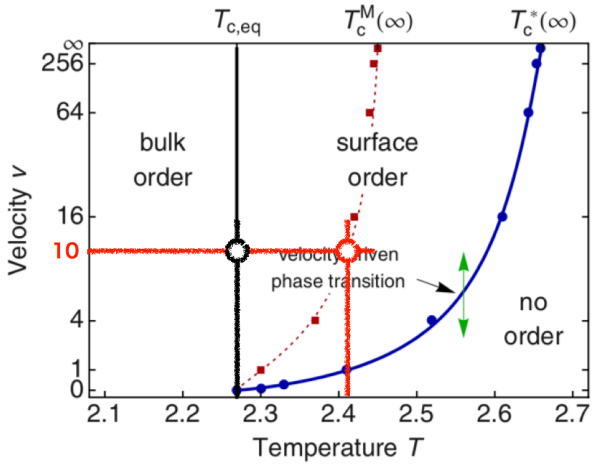

Figure 4.5: The non-equilibrium critical temperature $T_c^M(v) \simeq 2.40$ (the vertical red line) with the velocity $v \simeq 10$ and the equilibrium critical temperature $T_{c,eq} \simeq 2.27$ (the vertical black line) in the phase diagram of the two-dimensional non-equilibrium Ising model obtained in Ref. [1]. Reprinted Fig. 15 with permission from A. Hucht, Phys. Rev. E **80**, 061138 (2009). Copyright (2018) by the American Physical Society.

$$f(L_z, T) := \lim_{L_x \to \infty} \frac{F(L_x, L_z, T)}{L_x}, \tag{4.1}$$

$$\epsilon(L_z, T) := \lim_{L_x \to \infty} \frac{E_b(L_x . L_z, T)}{L_x L_z}. \tag{4.2}$$

We use the aspect ratios of $L_x = 30 \times L_z, 40 \times L_z, 50 \times L_z$ with L_z fixed in order to check the convergence in the limit $L_x/L_z \to \infty$. Figures 4.6, 4.7, 4.8 and 4.9 respectively show the temperature dependence of the frictional force density and the energy density under each set of boundary conditions for each size of $L_z = 4, 8, 16, 32, 64$. We see the quantities $F(L_x, L_z, T)/L_x$ and $E(L_x, L_z, T)/L_x$ for each set of boundary conditions have little dependence on L_x for sufficiently large size of L_x with each size of L_z.

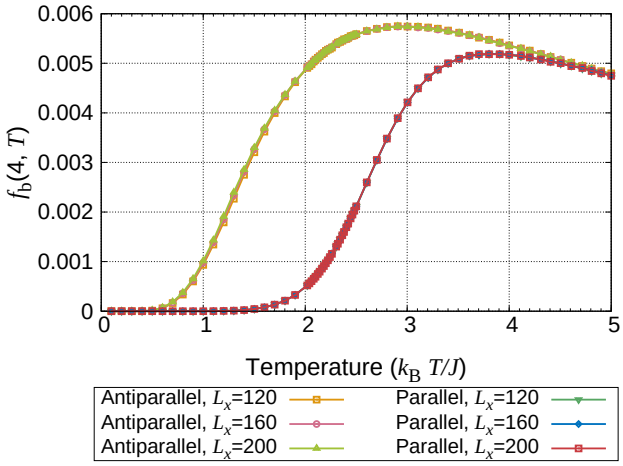

(a)

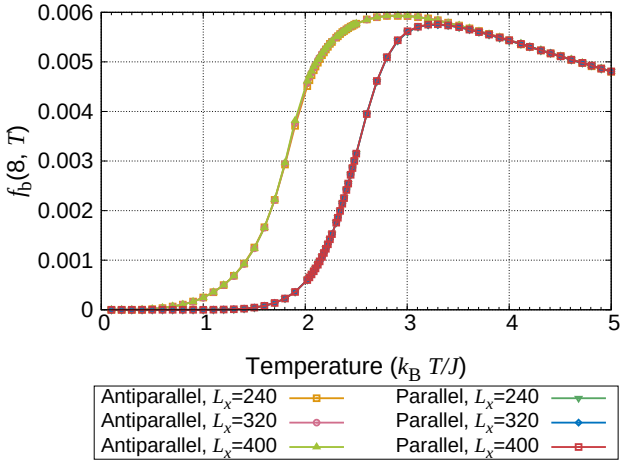

(b)

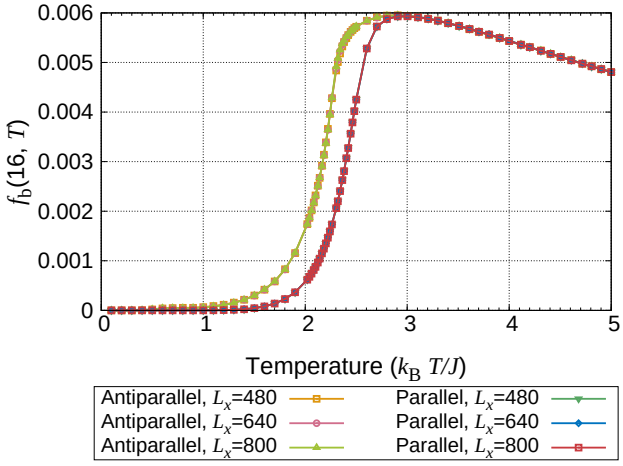

(c)

Figure 4.6: Each panel shows $F(L_x, L_z, T)/L_x$ against the temperature T: (a) $L_z = 4$; (b) $L_z = 8$; (c) $L_z = 16$.

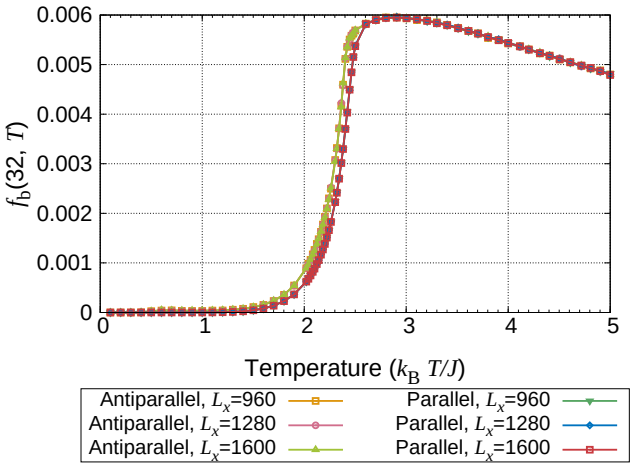

(a)

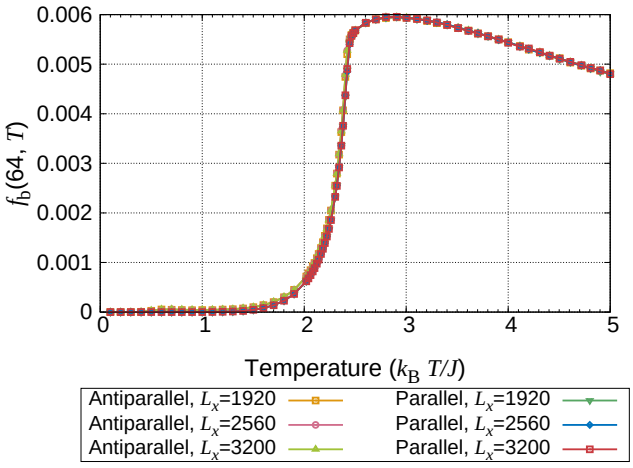

(b)

Figure 4.7: Each panel shows $F(L_x, L_z, T)/L_x$ against the temperature T: (a) $L_z = 32$; (b) $L_z = 64$.

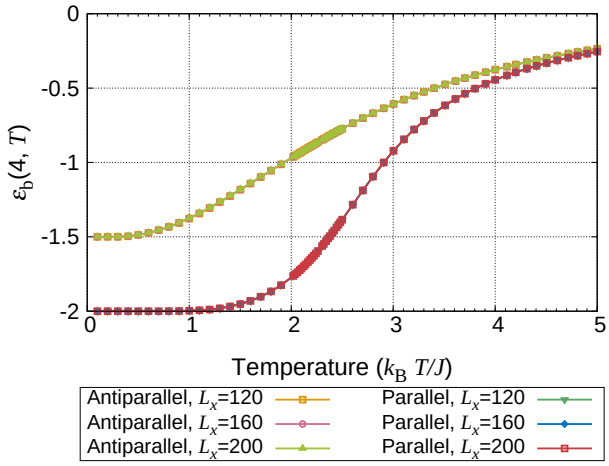

(a)

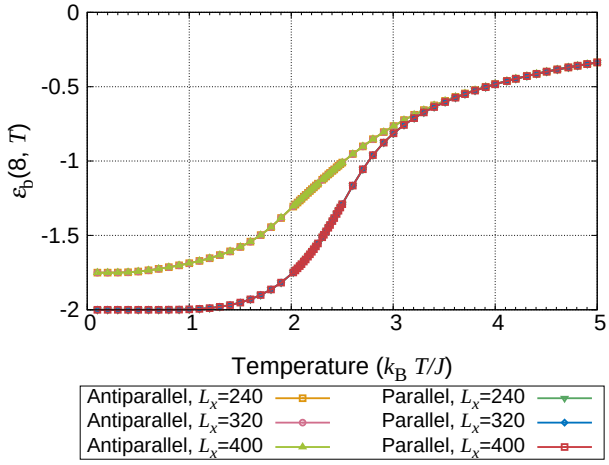

(b)

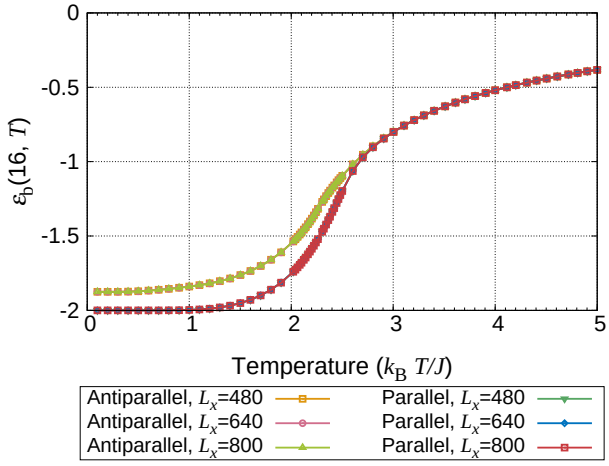

(c)

Figure 4.8: Each panel shows $E(L_x, L_z, T)/(L_x L_z)$ against the temperature T: (a) $L_z = 4$; (b) $L_z = 8$; (c) $L_z = 16$.

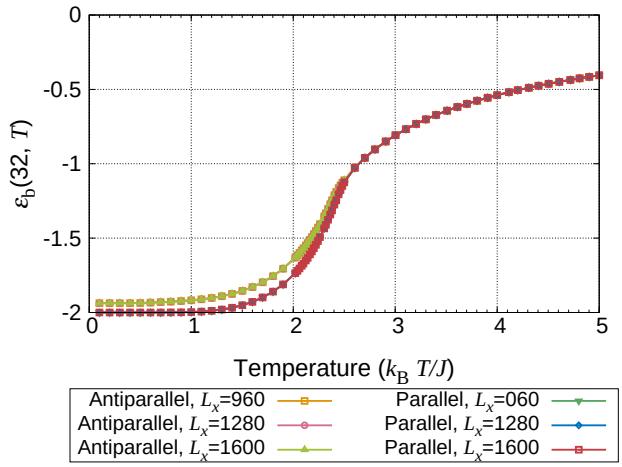

(a)

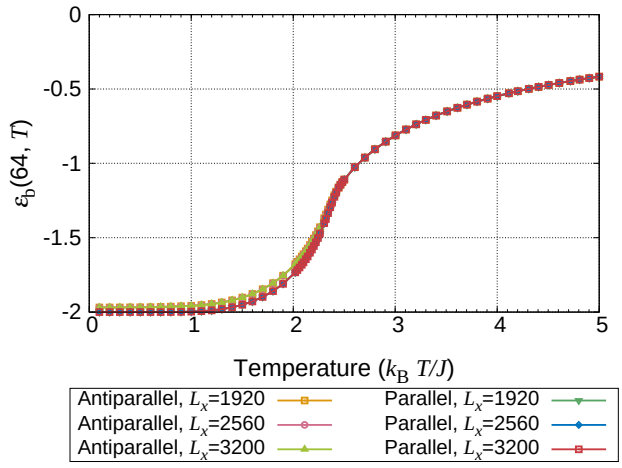

(b)

Figure 4.9: Each panel shows $E(L_x, L_z, T)/(L_x L_z)$ against the temperature T: (a) $L_z = 32$; (b) $L_z = 64$.

Chapter 5

Summary and Discussion

We investigated the effects of boundary conditions on the physical quantities by non-equilibrium Monte Carlo simulations. To summarize the present results, we found that the fixed boundary conditions have an effect on the magnetic friction as an effective field; the anti-parallel and the parallel boundary conditions have disordering and ordering effects, respectively. These effects emerge at the sliding boundary when the system behaves as a one-dimensional system, but vanish in the two-dimensional limit. The crossover between the one dimension and the two dimensions occurs below the size $L_z = 64$ in the limit $L_x \to \infty$.

In other words, if we set the size L_z much less (greater) than the correlation length $\xi_z(\beta)$ the system behaves as the one-dimensional (two-dimensional one). The two sets of boundary conditions, in particular, have maximum effects on the magnetic friction when the temperature of the system is near the boundary critical temperature and the system is sufficiently thin.

Thereby we propose to manipulate the magnetic friction by switching the one boundary conditions into the other near the boundary criticality. We can thus sharply increase and decrease the magnetic friction.

In order to be more precise, we should calculate the correlation length along the z direction $\xi_z(\beta)$. Its definition may be different from that of the equilibrium case because the homogeneity along the z direction is destroyed by the constant sliding motion.

For further analysis, it is worthwhile to determine critical exponents of the non-equilibrium phase transition. We can determine the critical exponent α of the bulk heat capacity $c(T)$ in Fig. 4.4 as well as the boundary heat capacity $c_{\mathrm{b}}(T)$ by further calculations. Similarly we can estimate the critical exponents ν, β and γ of the correlation length ξ_x along x direction, the boundary magnetization m_{b} and the boundary susceptibility $\chi_{\mathrm{b,abs}}$, respectively, by the methods in Ref. [1], which enables us to discuss a crossover from the one dimension to two dimensions by varying the size L_z.

According to Ref. [1], the scaling relation $2-\alpha = 2\beta+\gamma = d_{\mathrm{b}}\nu$ exists, where d_{b} denote the boundary dimension of the system for each bulk dimension and geometry. We can expect that the set of critical exponents exhibits a continuous change with the scaling relation holding.

The discussions on the experimental method of manipulating the magnetic friction and determination of the crossover point with more accuracy are applicable to any lattice system which can be simulated by our way. For more practical purposes, it is important

to study three-dimensional systems with two-dimensional surfaces. We intend to seek the way of manipulating the friction in three-dimensional systems for future work.

Appendix A

Analysis based on Stochastic Matrices

In this appendix, we prove the existence of the non-equilibrium stationary state in our model with sliding of arbitrary velocity. In the first section, we discuss the formulation in terms of stochastic matrices. In the following two sections, we prove based on Ref. [32] several facts for stochastic matrices, which ensures that almost all Monte Carlo simulations converge to a unique equilibrium state. In the last two sections, we propose a way to construct the matrix for both equilibrium cases and non-equilibrium stationary cases, and discuss the distributions of their eigenvalues in terms of the convergence.

A.1 A Simple Example: Stochastic Ising Model with N-spins

We now consider a matrix form of the stochastic process. For example, the one-dimensional Ising chain with N-spin has 2^N states. If we label each of the states by $i = 1, 2, \ldots, 2^N$, we can write the stochastic time evolution of the system by the existence probability $p_i(t)$ that the system is in the ith state at a time t and the transition probability T_{ij} such that the system in the jth state changes to the ith state.

We additionally define the conditional probability $\tilde{p}_{ij}(t)$ that the system in the jth state at a time t changes to the ith state at the next time $t+1$. Using the conditional probability, we can derive the relation between the existence probability $p_i(t)$ and the transition probability T_{ij} as

$$\tilde{p}_{ij}(t+1) = T_{ij} p_j(t) \quad \text{for } 1 \leq i, j \leq 2^N. \tag{A.1}$$

From a property of the probability, it should hold that $\sum_{i=1}^{2^N} p_i(t) = 1$ and $p_i(t) \geq 0$ ($i = 1, 2, \ldots, 2^N, t \in \mathbb{R}$). The conditional probability $\tilde{p}_{ij}(t)$ should also satisfy the condition that $\sum_{j=1}^{2^N} \tilde{p}_{ij}(t) = p_i(t+1)$ ($i = 1, 2, \ldots, 2^N, t \in \mathbb{R}$). Then we have

$$p_i(t+1) = \sum_{j=1}^{2^N} \tilde{p}_{ij}(t+1) = \sum_{j=1}^{2^N} T_{ij} p_j(t) \quad \text{for } 1 \leq i \leq 2^N,\ t \in \mathbb{R}. \tag{A.2}$$

In other words, the system can be described by the probability vector

$$\boldsymbol{p}(t) := {}^{\mathrm{t}}(p_1(t), p_2(t), \ldots, p_{2^N}(t)) \tag{A.3}$$

and the stochastic matrix $\hat{T} := (T_{ij})$ as

$$\boldsymbol{p}(t+1) = \hat{T}\boldsymbol{p}(t) \quad \text{for } t \in \mathbb{R}. \tag{A.4}$$

We have to consider such the matrix when we discuss the convergence to the stationary state or its uniqueness. These discussions are valid for general Ω-dimensional state spaces, and thus we denote the number of states by Ω from now on.

A.2 General Theory of Stochastic Matrices

In this section we discuss the conditions which ensure the convergence of a Monte Carlo simulation to a unique stationary state. We first define the stochastic matrix and discuss fundamental properties of the stochastic matrix. We next discuss a properties which result from an additional condition called *weak/strong connectivity*, and thereby show the existence and the uniqueness of a stationary state. We also see that we can construct a stochastic matrix which leads to any desired stationary state under the *detailed-balanced condition*.

From the condition $\sum_{i=1}^{\Omega} p_i(t) = 1$ and $p_i(t) \geq 0$ $(i = 1, 2, \ldots, \Omega, t \in \mathbb{R})$, we have a set of properties $\sum_{i=1}^{\Omega} T_{ij} = 1$, $T_{ij} \geq 0$ $(1 \leq i \leq \Omega)$. Any matrix with these conditions is called a *stochastic matrix* and shows the following interesting property:

Lemma A.2.1. Let $\hat{T}$ be a stochastic matrix. Then all absolute values of eigenvalue are less than or equal to unity. For any eigenvector $\boldsymbol{x} = {}^{\mathrm{t}}\{x_1, x_2, \ldots, x_\Omega\}$ which does *not* belong to the eigenvalue 1, it additionally holds that

$$\sum_{i=1}^{\Omega} x_j = 0. \tag{A.5}$$

We now define the vector $\boldsymbol{d} := {}^{\mathrm{t}}(1, 1, \ldots, 1)$ to prove all facts after this.

Proof. For any stochastic matrix $\hat{T}$, we have

$$\left({}^{\mathrm{t}}\hat{T}\boldsymbol{d}\right)_i = \sum_{j=1}^{\Omega} \left({}^{t}T\right)_{ij} d_j = \sum_{j=1}^{\Omega} T_{ji} d_j = \sum_{j=1}^{\Omega} T_{ji} = 1 \quad \text{for } i = 1, 2, \ldots, \Omega, \tag{A.6}$$

$$\iff \quad {}^{\mathrm{t}}\hat{T}\boldsymbol{d} = \boldsymbol{d}. \tag{A.7}$$

Therefore the matrix ${}^{\mathrm{t}}\hat{T}$ has at least an eigenvalue 1. The eigenequation for the matrix ${}^{\mathrm{t}}\hat{T}$ are rewritten as

$$\det\left[\lambda\hat{I}_\Omega - {}^{\mathrm{t}}\hat{T}\right] = \det\left[{}^{\mathrm{t}}\left(\lambda\hat{I}_\Omega - \hat{T}\right)\right] = \det\left[\lambda\hat{I}_\Omega - \hat{T}\right], \tag{A.8}$$

and then the set of eigenvalues of $\hat{T}$ is equal to that of ${}^{\mathrm{t}}\hat{T}$. Therefore the matrix $\hat{T}$ has at least an eigenvalue 1. A general eigenvalue equation of $\hat{T}$ can be written as

$$\hat{T}\boldsymbol{x}_n = \lambda_n \boldsymbol{x}_n, \tag{A.9}$$

where $\boldsymbol{x}_n = {}^{\mathrm{t}}(x_{n,1}, x_{n,2}, \ldots, x_{n,\Omega})$ is its eigenvector. We have

$$((\text{l.h.s of A.9}), \boldsymbol{d}) = (\hat{T}\boldsymbol{x}_\lambda, \boldsymbol{d}) = (\boldsymbol{x}_\lambda, {}^{\mathrm{t}}\hat{T}\boldsymbol{d}) = (\boldsymbol{x}_\lambda, \boldsymbol{d}), \tag{A.10}$$

$$((\text{r.h.s of A.9}), \boldsymbol{d}) = (\lambda\boldsymbol{x}_\lambda, \boldsymbol{d}) = \lambda(\boldsymbol{x}_\lambda, \boldsymbol{d}). \tag{A.11}$$

$$\iff \quad (1-\lambda)(\boldsymbol{x}_\lambda, \boldsymbol{d}) = 0 \quad \iff \quad \lambda = 1 \text{ or } (\boldsymbol{x}_\lambda, \boldsymbol{d}) = 0. \tag{A.12}$$

$$\implies \quad \sum_{i=1}^{\Omega} x_{\lambda,i} = 0 \quad \text{if } \lambda \neq 1. \tag{A.13}$$

We additionally define the vector $\boldsymbol{y}_\lambda := {}^{\mathrm{t}}(|x_{\lambda,1}|, |x_{\lambda,2}|, \ldots, |x_{\lambda,\Omega}|)$ for any λ. From the equation $\sum_{j=1}^{\Omega} T_{ij}x_{\lambda,j} = \lambda x_i (i = 1, 2, \ldots, \Omega)$, we have

$$\left|\sum_{j=1}^{\Omega} T_{ij}x_{\lambda,j}\right| \leq \sum_{j=1}^{\Omega} T_{ij}|x_{\lambda,j}| \quad (\because T_{ij} \geq 0 \quad \text{for } j = 1, 2, \ldots, \Omega) \tag{A.14}$$

$$= \left(\hat{T}\boldsymbol{y}_\lambda\right)_i \quad \text{for } i = 1, 2, \ldots, \Omega. \tag{A.15}$$

The left hand-side of (A.15) are rewritten as

$$\left|\sum_{j=1}^{\Omega} T_{ij}x_{\lambda,j}\right| = |\lambda x_{\lambda,j}| = |\lambda| \times |x_{\lambda,j}| = |\lambda| \times (\boldsymbol{y}_\lambda)_j\,, \tag{A.16}$$

and thus we have

$$|\lambda| \times (\boldsymbol{y}_\lambda)_j \leq \left(\hat{T}\boldsymbol{y}_\lambda\right)_i\,, \tag{A.17}$$

$$\iff \quad |\lambda| \times (\boldsymbol{y}_\lambda, \boldsymbol{d}) \leq \left(\hat{T}\boldsymbol{y}_\lambda, \boldsymbol{d}\right) = \left(\boldsymbol{y}_\lambda, {}^{\mathrm{t}}\hat{T}\boldsymbol{d}\right) = (\boldsymbol{y}_\lambda, \boldsymbol{d})\,, \tag{A.18}$$

$$\iff \quad |\lambda| \leq 1. \tag{A.19}$$

□

Definition A.2.1. For an arbitrary $1 \leq i, j \leq \Omega$, if there exists an $n(i,j) > 0$ such that

$$\left(\hat{T}^{n(i,j)}\right)_{ij} > 0, \tag{A.20}$$

the matrix $\hat{T}$ is called *weakly connected*. Note that for any $n' > n(i,j)$ it does *not* follow that $\left(\hat{T}^{n'}\right)_{ij} > 0$.

We limit the class of stochastic matrices to that of weakly connected ones from now on. To make the proofs of the theorems below easier, we also define the matrix $\hat{\mathcal{T}}_\epsilon$ $(\epsilon > 0)$ and discuss its properties. Denoting the maximum value of $n(i,j)$ by $n_{\max} := \max_{1 \leq i,j \leq \Omega}[n(i,j)]$ and defining the matrix $\hat{\mathcal{T}}_\epsilon := \left(\hat{I}_\Omega + \epsilon\hat{T}\right)^{n_{\max}}$, we have

$$\left(\hat{\mathcal{T}}_\epsilon\right)_{ij} = \left(\left(\hat{I}_\Omega + \epsilon\hat{T}\right)^{n_{\max}}\right)_{ij} = \sum_{k=1}^{n_{\max}} \binom{n_{\max}}{k} \left(\hat{I}_\Omega^k \left(\epsilon\hat{T}\right)^{n_{\max}-k}\right)_{ij} \tag{A.21}$$

$$= \sum_{k=1}^{n_{\max}} \binom{n_{\max}}{k} \epsilon^{n_{\max}-k} \left(\hat{T}^{n_{\max}-k}\right)_{ij} \geq 0 \quad (\because T_{ij} > 0) \quad \text{for } 1 \leq i, j \leq \Omega. \tag{A.22}$$

For the eigenvector $\boldsymbol{x}_1 = {}^{\mathrm{t}}(x_{1,1}, x_{1,2}, \ldots, x_{1,\Omega})$, which belongs to the eigenvalue 1, it holds that

$$\hat{\mathcal{T}}_\epsilon \boldsymbol{x}_1 = \sum_{k=1}^{n_{\max}} \binom{k}{n_{\max}} \epsilon^{n_{\max}-k} \hat{T}^{n_{\max}} \boldsymbol{x}_1 \tag{A.23}$$

$$= \sum_{k=1}^{n_{\max}} \binom{k}{n_{\max}} \epsilon^{n_{\max}-k} \boldsymbol{x}_1 \tag{A.24}$$

$$= (1+\epsilon)^{n_{\max}} \boldsymbol{x}_1, \tag{A.25}$$

and each component is

$$\sum_{j=1}^{\Omega} \left(\hat{\mathcal{T}}_\epsilon\right)_{ij} x_{1,j} = (1+\epsilon)^{n_{\max}} x_{1,i} \quad \text{for } i = 1, 2, \ldots, \Omega. \tag{A.26}$$

Lemma A.2.2. We can decompose the vector into a phase factor and a positive vector as follows:

$$\boldsymbol{x}_1 = \mathrm{e}^{i\theta} \boldsymbol{u}_1, \tag{A.27}$$

where θ is the phase and $\boldsymbol{u}_1$ is the vector with all positive components.

Proof. If components of the vector $\boldsymbol{x}_1$ are *not* common such that $\sum_{i=1}^{\Omega} |x_{1,i}| > |\sum_{i=1}^{\Omega} x_{1,i}|$ holds, we have

$$\left| \sum_{j=1}^{\Omega} \left(\hat{\mathcal{T}}_\epsilon\right)_{ij} x_{1,j} \right| < \sum_{j=1}^{\Omega} \left(\hat{\mathcal{T}}_\epsilon\right)_{ij} |x_{1,j}| = (1+\epsilon)^{n_{\max}} |x_{1,i}|. \tag{A.28}$$

On the other hand, the row-wise sum of the matrix $\hat{\mathcal{T}}_\epsilon$ are

$$\sum_{i=1}^{\Omega} \left(\hat{\mathcal{T}}_\epsilon\right)_{ij} = \sum_{k=1}^{n_{\max}} \binom{k}{n_{\max}} \epsilon^{n_{\max}-k} \sum_{i=1}^{\Omega} \left(\hat{T}^{n_{\max}-k}\right)_{ij} = (1+\epsilon)^{n_{\max}}. \tag{A.29}$$

Then we have

$$\sum_{i=1}^{\Omega} \sum_{j=1}^{\Omega} \left(\hat{\mathcal{T}}_\epsilon\right)_{ij} |x_{1,j}| = (1+\epsilon)^{n_{\max}} \sum_{j=1}^{\Omega} |x_{1,j}| > (1+\epsilon)^{n_{\max}} \sum_{i=1}^{\Omega} |x_{1,i}|, \tag{A.30}$$

but it is the contradiction caused from our assumption $\sum_{i=1}^{\Omega} |x_{1,i}| > |\sum_{i=1}^{\Omega} x_{1,i}|$. Furthermore the left-hand side of (A.26) is positive because $n_{\max}$ is the maximum value of $n(i,j)$, and therefore the right-hand side is also positive $x_{1,i} > 0$ $(i = 1, 2, \ldots, \Omega)$. □

Lemma A.2.3. The eigenspace of the matrix $\hat{\mathcal{T}}_\epsilon$, which belongs to the eigenvalue 1, is *one-dimensional*.

Proof. If we have two different eigenvectors which belongs to the eigenvalue 1, we can write their eigenequations by two different *positive vectors* as

$$\hat{T} \boldsymbol{u}_1 = \boldsymbol{u}_1, \tag{A.31}$$

$$\hat{T} \boldsymbol{v}_1 = \boldsymbol{v}_1. \tag{A.32}$$

For their any linear superposition, we also have

$$\hat{T}(\boldsymbol{u}_1 + t\boldsymbol{v}_1) = \boldsymbol{u}_1 + t\boldsymbol{v}_1, \quad \text{for any } t \in \mathbb{R}. \tag{A.33}$$

If two eigenvectors $\boldsymbol{u}_1$ and $\boldsymbol{v}_1$ are not parallel to each other, we can make a non-trivial vector with a certain value of t such that $(\boldsymbol{u}_1 + t\boldsymbol{v}_1)_l = 0$ for an lth element. However it is the contradiction with the fact $x_{1,i} > 0$ $(i = 1, 2, \ldots, \Omega)$. Therefore we have no eigenspaces more than one which belongs to the eigenvalue 1. □

Definition A.2.2. If there exists a number $N_0 > 0$ such that

$$\left(\hat{T}^{N_0}\right)_{ij} > 0 \tag{A.34}$$

for an arbitrary $1 \leq i, j \leq \Omega$, the matrix $\hat{T}$ is called *strongly connected*.

We additionally limit the class of stochastic matrices to that of strongly connected ones from now on.

Theorem A.2.4. Unity is the only eigenvalue of absolute value 1.

Proof. We now have $\hat{T}^m \boldsymbol{u}_n = {\lambda_n}^m \boldsymbol{u}_n$, where $\boldsymbol{u}_n = {}^{\mathrm{t}}(u_{n,1}, u_{n,2}, \ldots, u_{n,\Omega})$ is the eigenvector which belongs to an eigenvalue λ. Their components are written as

$$\sum_{j=1}^{\Omega} \left(\hat{T}^n\right)_{ij} u_{\lambda,j} = \lambda^n \boldsymbol{u}_{\lambda,i} \quad \text{for } i = 1, 2, \ldots, \Omega. \tag{A.35}$$

We can divide conditions for λ into the following two cases:

Case 1: $\sum_{i=1}^{\Omega} |u_{\lambda,i}| > |\sum_{i=1}^{\Omega} u_{\lambda,i}|$**,**
We have

$$\sum_{j=1}^{\Omega} \left(\hat{T}^n\right)_{ij} |u_{\lambda,j}| > |\sum_{j=1}^{\Omega} \left(\hat{T}^n\right)_{ij} u_{\lambda,j}| = |\lambda^n| \times |u_{\lambda,i}|, \quad \text{for } i = 1, 2, \ldots, \Omega. \tag{A.36}$$

$$\Longleftrightarrow \quad |\lambda^n| < 1 \quad \Longleftrightarrow \quad |\lambda| < 1. \tag{A.37}$$

Case 2: $\sum_{i=1}^{\Omega} |u_{\lambda,i}| = |\sum_{i=1}^{\Omega} u_{\lambda,i}|$**.**
We have

$$\sum_{i=1}^{\Omega} \sum_{j=1}^{\Omega} \left(\hat{T}^n\right)_{ij} u_{\lambda,j} = \sum_{j=1}^{\Omega} u_{\lambda,j} = \lambda^n \sum_{i=1} u_{\lambda,i}. \tag{A.38}$$

$$\Longleftrightarrow \quad \lambda^n = 1 \quad \left(\because \boldsymbol{u}_\lambda \neq \boldsymbol{0}, u_{\lambda,i} \geq 0 \Rightarrow \sum_{i=1}^{\Omega} u_{\lambda,i} > 0 \right). \tag{A.39}$$

Thus the eigenvalue 1 is the only eigenvalue of absolute value 1. □

Lemma A.2.5. The vector $\lim_{N\to\infty} \hat{T}^N \boldsymbol{r} = \boldsymbol{0}$ for any $\boldsymbol{r} \in \mathbb{C}$ is orthogonal to $\boldsymbol{d}$.

Proof. For an arbitrary vector $\boldsymbol{r}$, we can decompose it into its real and imaginary parts as $\boldsymbol{r} = \boldsymbol{r}_{\mathrm{R}} + i\boldsymbol{r}_{\mathrm{I}}$. Since the condition $(\boldsymbol{r}, \boldsymbol{d}) = 0$ is equivalent to $\sum_{i=1}^{\Omega} r_i = 0$, we have

$$\sum_{j \in I_+} r_j + \sum_{j \in I_-} r_j = 0, \tag{A.40}$$

where $I_\pm := \{j \mid r_j \gtrless 0, 1 \le j \le \Omega\}$. Note that $\sum_{j \in I_+} r_j = \sum_{j \in I_-} |r_j|$. Thus we have

$$\sum_{j \in I_+} r_j = \sum_{j \in I_-} |r_j| = \|\boldsymbol{r}\|_1 / 2. \tag{A.41}$$

Since $\hat{T}$ is strongly connected, there is an integer N_0 such that $\left(\hat{T}^{N_0}\right)_{ij} > 0$ for an arbitrary $1 \le i, j \le \Omega$. For N_0, we have

$$\begin{aligned}
\left(\hat{T}^{N_0}\boldsymbol{r}\right) = \sum_{j=1}^{\Omega} \left(\hat{T}^{N_0}\right)_{ij} r_j &= \sum_{j \in I_+} \left(\hat{T}^{N_0}\right)_{ij} r_j - \sum_{j \in I_-} \left(\hat{T}^{N_0}\right)_{ij} |r_j| && \text{(A.42)} \\
&= \sum_{j=1}^{\Omega} \left(\hat{T}^{N_0}\right)_{ij} r_j - 2 \sum_{j \in I_-} \left(\hat{T}^{N_0}\right)_{ij} |r_j| && \text{(A.43)} \\
&\le \sum_{j=1}^{\Omega} \left(\hat{T}^{N_0}\right)_{ij} r_j - 2\delta_{N_0} \sum_{j \in I_-} |r_j| && \text{(A.44)} \\
&= \sum_{j=1}^{\Omega} \left(\hat{T}^{N_0}\right)_{ij} r_j - \delta_{N_0} \|\boldsymbol{r}\|_1, && \text{(A.45)}
\end{aligned}$$

where $\delta_{N_0} := \min_{1 \le i,j \le \Omega} \left[\left(\hat{T}^{N_0}\right)_{ij}\right]$ for $i = 1, 2, \ldots, \Omega$. Note that there exists $\delta_{N_0} > 0$ for the strongly connected matrix $\hat{T}$. Similarly we have

$$\begin{aligned}
\left(\hat{T}^{N_0}\boldsymbol{r}\right) = \sum_{j=1}^{\Omega} \left(\hat{T}^{N_0}\right)_{ij} r_j &= \sum_{j \in I_+} \left(\hat{T}^{N_0}\right)_{ij} r_j - \sum_{j \in I_-} \left(\hat{T}^{N_0}\right)_{ij} |r_j| && \text{(A.46)} \\
&= 2 \sum_{j \in I_+} \left(\hat{T}^{N_0}\right)_{ij} r_j - \sum_{j=1}^{\Omega} \left(\hat{T}^{N_0}\right)_{ij} |r_j| && \text{(A.47)} \\
&\ge 2\delta_{N_0} \sum_{j \in I_+} r_j - \sum_{j=1}^{\Omega} \left(\hat{T}^{N_0}\right)_{ij} |r_j| && \text{(A.48)} \\
&= \delta_{N_0} \|\boldsymbol{r}\|_1 - \sum_{j=1}^{\Omega} \left(\hat{T}^{N_0}\right)_{ij} |r_j| \quad \text{for } i = 1, 2, \ldots, \Omega. && \text{(A.49)}
\end{aligned}$$

Combining them, we have

$$\left| \left(\hat{T}^{N_0}\boldsymbol{r}\right) \right| \le \sum_{j=1}^{\Omega} \left(\hat{T}^{N_0}\right)_{ij} |r_j| - \delta_{N_0} \|\boldsymbol{r}\|_1 \quad \text{for } i = 1, 2, \ldots, \Omega, \tag{A.50}$$

and then it holds that

$$\|\hat{T}^{N_0}\boldsymbol{r}\|_1 = \sum_{i=1}^{\Omega} |\left(\hat{T}^{N_0}\boldsymbol{r}\right)_i| \leq \sum_{j=1}^{\Omega} |r_j| - N_0\delta_{N_0}\|\boldsymbol{r}\|_1 = (1 - N\delta_{N_0})\|\boldsymbol{r}\|_1. \tag{A.51}$$

The vector $\hat{T}^{N_0}\boldsymbol{r}$ is also orthogonal to the vector $\boldsymbol{d}$:

$$\left(\hat{T}^{N_0}\boldsymbol{r}, \boldsymbol{d}\right) = \left(\boldsymbol{r}, {}^{\mathrm{t}}\left(\hat{T}^{N_0}\right)\boldsymbol{d}\right) = \left(\boldsymbol{r}, \left({}^{\mathrm{t}}\hat{T}\right)^{N_0}\boldsymbol{d}\right) = (\boldsymbol{r}, \boldsymbol{d}) = 0. \tag{A.52}$$

Then, for any positive integer l, we can repeat this discussion as

$$\|\hat{T}^{N_0 l}\boldsymbol{r}\|_1 \leq (1 - N_0\delta_{N_0})^l \|\boldsymbol{r}\|_1. \tag{A.53}$$

Since $N_0 > 0, \delta_{N_0} > 0$ and thus $1 - N_0\delta_{N_0} < 0$, we have

$$\lim_{l\to\infty}(1 - N_0\delta_{N_0})^l\|\boldsymbol{r}\|_1 = 0. \tag{A.54}$$

$$\iff \quad \lim_{l\to\infty}\|\hat{T}^{N_0 l}\boldsymbol{r}\|_1 = 0. \tag{A.55}$$

Thus, for an arbitrary positive integer N, we have

$$\lim_{N\to\infty}\|\hat{T}^{N}\boldsymbol{r}\|_1 = 0. \tag{A.56}$$

□

Lemma A.2.6. We can write any vector $\boldsymbol{x}$ as the superposition of $\boldsymbol{u}_1$ and $\boldsymbol{r}$.

Proof. Defining the coefficient $c_{1,\boldsymbol{x}} := (\boldsymbol{x}, \boldsymbol{d})/(\boldsymbol{u}_1, \boldsymbol{d})$ and the vector $\boldsymbol{r}_{\boldsymbol{x}} := \boldsymbol{x} - c_{1,\boldsymbol{x}}\boldsymbol{u}_1$, we have

$$(\boldsymbol{r}_{\boldsymbol{x}}, \boldsymbol{d}) = (\boldsymbol{x}, \boldsymbol{d}) - \frac{(\boldsymbol{x}, \boldsymbol{d})}{(\boldsymbol{u}_1, \boldsymbol{d})}(\boldsymbol{u}_1, \boldsymbol{d}) = 0, \tag{A.57}$$

$$\boldsymbol{x} = c_{1,\boldsymbol{x}}(\boldsymbol{u}_1, \boldsymbol{d}) + \boldsymbol{r}_{\boldsymbol{x}}. \tag{A.58}$$

□

Theorem A.2.7. The limit $\lim_{N\to\infty}\hat{T}^N\boldsymbol{p}^{(0)}$ is independent of the initial vector $\boldsymbol{p}^{(0)}$:

$$\lim_{N\to\infty}\hat{T}^N\boldsymbol{p}^{(0)} = \frac{\boldsymbol{u}_1}{\|\boldsymbol{u}_1\|_1}, \tag{A.59}$$

where the vector $\boldsymbol{p}^{(0)} = {}^{\mathrm{t}}\left\{p_1^{(0)}, p_2^{(0)}, \ldots, p_\Omega^{(0)}\right\}$ is in the class of probability vectors normalized as $\sum_{i=1}^{\Omega} p_i^{(0)} = 1$.

Proof. From the theorem A.2.6, we have

$$\hat{T}^N\boldsymbol{p}^{(0)} = c_{1,\boldsymbol{p}^{(0)}}\hat{T}^N\boldsymbol{u}_1 + \hat{T}^N\boldsymbol{r}_{\boldsymbol{p}^{(0)}} = c_{1,\boldsymbol{p}^{(0)}}\boldsymbol{u}_1 + \hat{T}^N\boldsymbol{r}_{\boldsymbol{p}^{(0)}}. \tag{A.60}$$

Its limit $N \to \infty$ is taken as

$$\lim_{N\to\infty}\hat{T}^N\boldsymbol{p}^{(0)} = c_{1,\boldsymbol{p}^{(0)}}\boldsymbol{u}_1 + \lim_{N\to\infty}\hat{T}^N\boldsymbol{r}_{\boldsymbol{p}^{(0)}} = c_{1,\boldsymbol{p}^{(0)}}\boldsymbol{u}_1. \tag{A.61}$$

Using the matrix $\hat{A} := \boldsymbol{u}_1{}^{\mathrm{t}}\boldsymbol{d}/(\boldsymbol{u}_1, \boldsymbol{d})$, we have

$$\left(\hat{A}\boldsymbol{p}^{(0)}\right)_i = \sum_{j=1}^{\Omega} \frac{(\boldsymbol{u}_1)_i}{(\boldsymbol{u}_1, \boldsymbol{d})} \left(\boldsymbol{p}^{(0)}\right)_j = \left(\boldsymbol{p}^{(0)}, \boldsymbol{d}\right) \frac{(\boldsymbol{u}_1)_i}{(\boldsymbol{u}_1, \boldsymbol{d})}, \quad \text{for } i = 1, 2, \ldots, \Omega. \tag{A.62}$$

It leads to

$$\hat{A}\boldsymbol{p}^{(0)} = \frac{(\boldsymbol{u}_1)_i}{(\boldsymbol{u}_1, \boldsymbol{d})}\boldsymbol{p}^{(0)} = c_{1,\boldsymbol{p}^{(0)}}\boldsymbol{p}^{(0)}. \tag{A.63}$$

The limit $N \to \infty$ for $\hat{T}^N\boldsymbol{p}^{(0)}$ is rewritten by a simple multiplication as follows:

$$\lim_{N\to\infty} \hat{T}^N\boldsymbol{p}^{(0)} = \frac{\boldsymbol{u}_1{}^{\mathrm{t}}\boldsymbol{d}}{(\boldsymbol{u}_1, \boldsymbol{d})}\boldsymbol{p}^{(0)}. \tag{A.64}$$

The expression (A.64) lead to the relation $\lim_{N\to\infty} \hat{T}^N\boldsymbol{p}^{(0)} = \boldsymbol{u}_1/\|\boldsymbol{u}_1\|_1$. Indeed it holds that

$$\frac{\boldsymbol{u}_1{}^{\mathrm{t}}\boldsymbol{d}}{(\boldsymbol{u}_1, \boldsymbol{d})} \left(\boldsymbol{p}^{(0)}\right)_i = \frac{\sum_{j=1}^{\Omega} (\boldsymbol{u}_1)_i (\boldsymbol{d})_j \left(\boldsymbol{p}^{(0)}\right)_j}{(\boldsymbol{u}_1, \boldsymbol{d})} = \frac{u_{1,i}}{\|\boldsymbol{u}_1\|_1}, \tag{A.65}$$

and thus we have

$$\lim_{N\to\infty} \hat{T}^N\boldsymbol{p}^{(0)} = \frac{\boldsymbol{u}_1}{\|\boldsymbol{u}_1\|_1}. \tag{A.66}$$

□

Once we get a strongly connected stochastic matrix $\hat{T}$, its stationary distribution $\boldsymbol{u}_1/\|\boldsymbol{u}_1\|_1$ is determined independently of the initial distribution.

A.3 Construction of the Stochastic Matrix based on the Detailed Balanced Condition

On the other hand, we can also construct the inverse discussion. This means the *construction* of the matrix $\hat{T}'$ with a *desired* stationary distribution $\boldsymbol{p}'$. We can formulate such a procedure using the *detailed-balanced condition* as follows.

Definition A.3.1. The matrix $\hat{T}'$ satisfies the detailed-balanced condition if it holds that

$$T'_{ij}p'_j = T'_{ji}p'_i \quad \text{for } 1 \leq i, j \leq \Omega \tag{A.67}$$

for the stationary distribution $\boldsymbol{p}' = {}^{\mathrm{t}}(p'_1, p'_2, \ldots, p'_\Omega)$.

This property is simplified by summing over the subscription i as follows

$$\sum_{i=1}^{\Omega} T'_{ij}p'_j = p'_j = \sum_{i=1}^{\Omega} T'_{ji}p'_i = \left(\hat{T}\boldsymbol{p}'\right)_j, \quad \text{for } j = 1, 2, \ldots, \Omega. \tag{A.68}$$

Then if the detailed-balanced condition holds for a matrix $\hat{T}'$, the corresponding vector $\boldsymbol{p}'$ is the fixed point of the matrix $\hat{T}'$. Thus in order to obtain the matrix $\hat{T}'$ which leads any distribution $\boldsymbol{p}^{(0)}$ to the desired distribution $\boldsymbol{p}'$, we only have to construct each element T'_{ij} of the matrix according to the condition (A.67) and make the matrix strongly connected.

In Monte Carlo simulations of statistical mechanics, we calculate the equilibrium distribution $\boldsymbol{p}_{\mathrm{eq}}(\beta)$ at an inverse temperature β using an initial state i_0 and a rule of the stochastic process $i \to j \to j' \to \dots$. We can regard the matrix construction method as a set of the stochastic process $i_0 \to j \to j' \to \dots$ over all possible states $i_0 = 1, 2, \dots, \Omega$.

The condition (A.67) or

$$\frac{T_{ij}}{T_{ji}} = \frac{p_i}{p_j} \tag{A.69}$$

is not sufficient to determine a concrete form of the matrix $\hat{T}$ and thus in general there is a degree of freedom in the form of $\hat{T}$. For Monte Carlo simulations of equilibrium statistical mechanics, this freedom also remains as follows:

$$\frac{T_{ij}(\beta)}{T_{ji}(\beta)} = \frac{p_i(\beta)}{p_j(\beta)} = \mathrm{e}^{-\beta(E_i - E_j)} \quad \text{for } 1 \le i, j \le \Omega, \tag{A.70}$$

where $T_{ij}(\beta)$ and $p_i(\beta)$ are the matrix corresponding to a simulation and the probability that the ith state emerges, respectively, at a fixed inverse temperature β. Nonetheless the relation (A.70) is important in that the rate of transition probabilities is always given by the difference of energies $\{E_1, E_2, \dots, E_\Omega\}$, and thus we do *not* have to calculate the exact values of $\tilde{p}_i(\beta) := \exp\left[-\beta E_i\right] / Z(\beta)$, where $Z(\beta) := \sum_i \exp\left[-\beta E_i\right]$.

If we use the Metropolis algorithm for the N-spin system, each element of the matrix $T_{ij}(\beta)$ is written as follows.

$$T_{ij}(\beta) = \begin{cases} \frac{1}{N} \min\left[1, \mathrm{e}^{-\beta(E_i - E_j)}\right] & \text{for states } i, j \text{ mutually reacheable by a single flip,} \\ 0 & \text{for states } i, j \textit{ not} \text{ mutually reacheable by a single flip.} \end{cases} \tag{A.71}$$

The factor $1/N$ describes the random selection of a spin to flip.

We call the matrix with the condition (A.71) the *Metropolis matrix* and denote it by M_{ij} from now on.

Metropolis matrices generally have few non-zero elements because of not taking transitions between all energy eigenstates into account. Thus the Monte Carlo simulation with the Metropolis rate is very simple, but the convergence is not trivial. In the following subsections, we show the convergence for quite limited cases using the strong connectivity of the stochastic matrix.

A.3.1 Metropolis Matrix for the Model of the Size 3×2

We construct the Metropolis matrix $\hat{M}(\beta)$ for the model of size $L_x = 3$, $L_z = 2$ in a concrete form and verify that all elements of the sixth power of the matrix are non-zero. By the fact, we can see the existence of its unique stationary state in the long-time limit . In addition we investigate the distribution of the eigenvalues of $\hat{M}(\beta)$ for several temperatures and verify that the matrix $\hat{M}(\beta)$ has only one eigenvalue of unity and all other eigenvalues are inside the unit circle on the complex plane except for the case $\beta = 0$; see Fig. A.2.

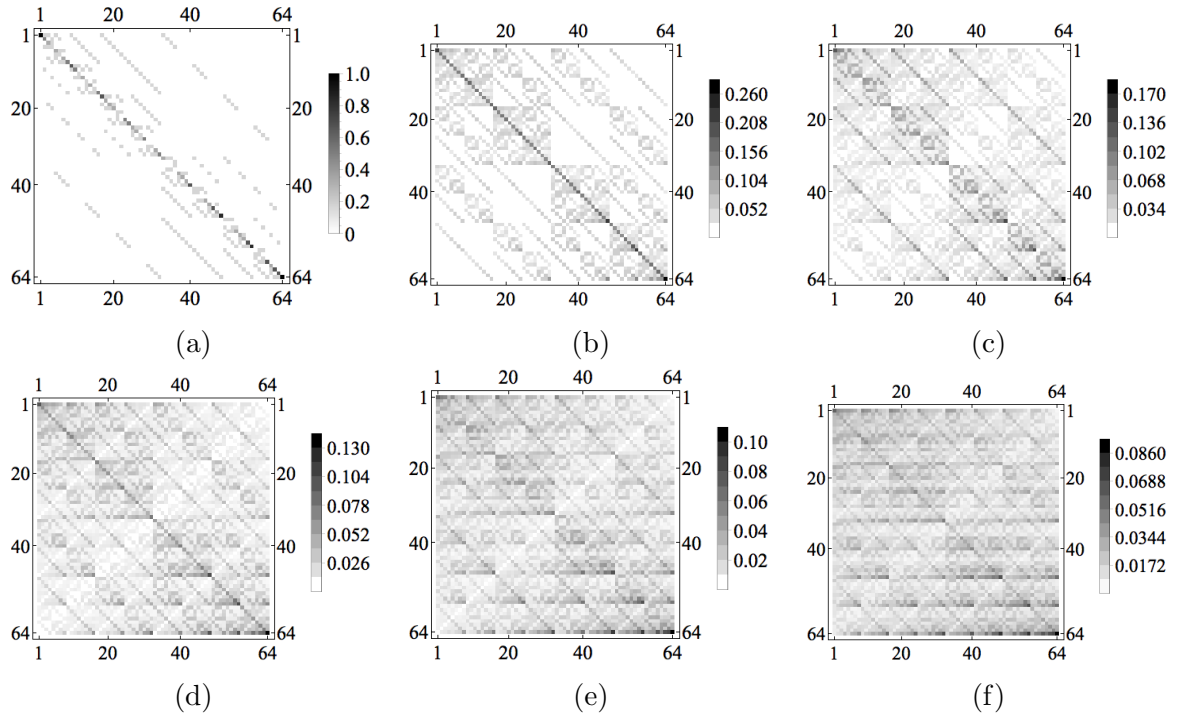

Figure A.1: The array plots of powers of $\hat{M}(\beta)$ of size $L_x = 3, L_z = 2$ and at the temperature $T = 10$: (a) $\hat{M}(\beta)$; (b) $\left(\hat{M}(\beta)\right)^2$; (c) $\left(\hat{M}(\beta)\right)^3$; (d) $\left(\hat{M}(\beta)\right)^4$; (e) $\left(\hat{M}(\beta)\right)^5$; (f) $\left(\hat{M}(\beta)\right)^6$.

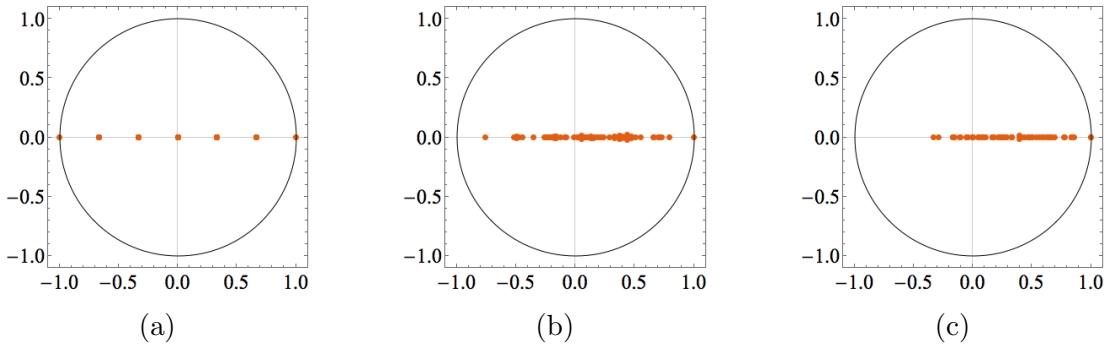

Figure A.2: The distributions of eigenvalues for $\hat{M}(\beta)$: (a) $\beta \to +0$; (b) $\beta = 0.1$; (c) $\beta \to +\infty$.

Bibliography

[1] A. Hucht, Phys. Rev. E **80**, 061138 (2009).

[2] Y. Hidaka, S. Kai, and H. Matsukawa, *Pattern Dynamicss of Liquid Crystals; Science of Sliding Frictions* (Baifukan, 2009), pp. 95–223.

[3] T. Bouhacina, J. P. Aimé, S. Gauthier, D. Michel, and V. Heroguez, Phys. Rev. B **56**, 7694 (1997).

[4] E. Gnecco, R. Bennewitz, T. Gyalog, C. Loppacher, M. Bammerlin, E. Meyer, and H.-J. Güntherodt, Phys. Rev. Lett. **84**, 1172 (2000).

[5] J. Chen, I. Ratera, J. Y. Park, and M. Salmeron, Phys. Rev. Lett. **96**, 236102 (2006).

[6] M. H. Müser, Phys. Rev. B **84**, 125419 (2011).

[7] O. M. Braun and M. Peyrard, Phys. Rev. E **83**, 046129 (2011).

[8] K. Hashiguchi, M. Ueno, T. Kuwayama, N. Suzuki, S. Yonemura, and N. Yoshikawa, Proc. R. Soc. A Math. Phys. Eng. Sci. **472**, 20160212 (2016).

[9] Q. Li, Y. Dong, D. Perez, A. Martini, and R. W. Carpick, Phys. Rev. Lett. **106**, 1 (2011).

[10] M. Bhattacharya, A. Dutta, and P. Barat, Phys. Rev. B **87**, 214107 (2013).

[11] L. Xu, T. B. Ma, Y. Z. Hu, and H. Wang, Nanotechnology **22**, 2 (2011).

[12] L. Jansen, H. H??lscher, H. Fuchs, and A. Schirmeisen, Phys. Rev. Lett. **104**, 1 (2010).

[13] F. J. Elmer, Phys. Rev. E **50**, 4470 (1994).

[14] Z. Zheng, B. Hu, and G. Hu, Phys. Rev. B **58**, 5453 (1998).

[15] M. Bhattacharya, A. Dutta, and P. Barat, Phys. Rev. B **87**, 214107 (2013).

[16] C. L. Wang, W. S. Duan, X. R. Hong, and J. M. Chen, Appl. Phys. Lett. **93** (2008) 10.1063/1.3003862.

[17] A. Benassi, M. Ma, M. Urbakh, and A. Vanossi, Sci. Rep. **5**, 1 (2015).

[18] A. Dayo, W. Alnasrallah, and J. Krim, Phys. Rev. Lett. **80**, 1690 (1998).

[19] T. Novotný and B. Velický, Phys. Rev. Lett. **83**, 4112 (1999).

[20] Y. Qi, J. Y. Park, B. L. M. Hendriksen, D. F. Ogletree, and M. Salmeron, Phys. Rev. B **77**, 184105 (2008).

[21] D. Kadau, A. Hucht, and D. E. Wolf, Phys. Rev. Lett. **101**, 137205 (2008).

[22] C. Fusco, D. E. Wolf, and U. Nowak, Phys. Rev. B **77**, 174426 (2008).

[23] M. P. Magiera, S. Angst, A. Hucht, and D. E. Wolf, Phys. Rev. B **84**, 212301 (2011).

[24] B. Wolter, Y. Yoshida, A. Kubetzka, S.-W. Hla, K. von Bergmann, and R. Wiesendanger, Phys. Rev. Lett. **109**, 116102 (2012).

[25] F. Iglói, M. Pleimling, and L. Turban, Phys. Rev. E **83**, 041110 (2011).

[26] A. Hucht and S. Angst, Europhys. Lett. **100**, 20003 (2012).

[27] S. Angst, A. Hucht, and D. E. Wolf, Phys. Rev. E **85**, 051120 (2012).

[28] L. Li and M. Pleimling, Phys. Rev. E **93**, 042122 (2016).

[29] M. P. Magiera, L. Brendel, D. E. Wolf, and U. Nowak, Europhys. Lett. **87**, 26002 (2009).

[30] M. P. Magiera, L. Brendel, D. E. Wolf, and U. Nowak, Europhys. Lett. **95**, 17010 (2011).

[31] R. J. Glauber, J. Math. Phys. **4**, 294 (1963).

[32] T. Hara, *Lecture Note for Mathematics (in Japanese)* (http://www2.math.kyushu-u.ac.jp/~hara/lectures/11/tokuronA3-ho.pdf, 2011), pp. 1–42.